Inorganic Chemistry
Award Article

Inorg. Chem. **2009**, *48*, 10001–10017 **10001**
DOI: 10.1021/ic901328v

Chemistry of Personalized Solar Energy

Daniel G. Nocera*

Department of Chemistry, 6-335, Massachusetts Institute of Technology (MIT), 77 Massachusetts Avenue, Cambridge, Massachusetts 02139-4307

Received July 9, 2009

Personalized energy (PE) is a transformative idea that provides a new modality for the planet's energy future. By providing solar energy to the individual, an energy supply becomes secure and available to people of both legacy and nonlegacy worlds and minimally contributes to an increase in the anthropogenic level of carbon dioxide. Because PE will be possible only if solar energy is available 24 h a day, 7 days a week, the key enabler for solar PE is an inexpensive storage mechanism. HY (Y = halide or OH^-) splitting is a fuel-forming reaction of sufficient energy density for large-scale solar storage, but the reaction relies on chemical transformations that are not understood at the most basic science level. Critical among these are *multielectron transfers* that are *proton-coupled* and involve the *activation of bonds in energy-poor substrates*. The chemistry of these three italicized areas is developed, and from this platform, discovery paths leading to new hydrohalic acid- and water-splitting catalysts are delineated. The latter water-splitting catalyst captures many of the functional elements of photosynthesis. In doing so, a highly manufacturable and inexpensive method for solar PE storage has been discovered.

1. Introduction

Global energy need will roughly double by midcentury and triple by 2100 because of the rising standards of living of a growing world population.[1] Most of that demand is driven by 3 billion low-energy users in the nonlegacy world and by 3 billion people yet to inhabit the planet over the next half-century. To hold atmospheric carbon dioxide (CO_2) levels to even twice their preanthropogenic values and at the same time to meet the increased energy demand of these 6 billion additional energy users will require invention, development, and deployment of carbon-neutral energy on a scale commensurate with, or larger than, the entire present-day energy supply from all sources combined.[2−4] The capture and storage of solar energy at the individual level—personalized solar energy—drives inextricably toward the heart of this energy challenge by addressing the triumvirate of secure, carbon-neutral, and plentiful energy.[5] Because energy use scales with wealth,[1] point-of-use solar energy will put individuals, in the smallest village in the nonlegacy world and in the largest city of the legacy world, on a more level playing field. Moreover, personalized energy (PE) is secure because it is highly distributed and the individual controls the energy on which she/he lives. Finally, the possibility of generating terawatts of carbon-free energy may be realized by making solar PE available to the 6 billion new energy users by high-throughput manufacturing. Notwithstanding, current options to harness and store solar energy at the individual level are too expensive to be implemented, especially in a nonlegacy world. The imperative to science is to develop new materials, reactions, and processes that enable the capture, conversion, and storage of solar energy to be sufficiently inexpensive to penetrate global energy markets.[3] Most, if not all, of these materials and processes entail a metallic element. Accordingly, the subject of inorganic chemistry is especially germane to delivering solar PE to our planet.[6]

Because society relies on a continuous energy supply and solar energy is diurnal, a key enabler for PE is an inexpensive storage mechanism. Most current methods of solar storage are characterized by low-energy densities, and consequently they present formidable challenges for large-scale solar PE implementation. The energy densities of compressed air (∼0.5 MJ/kg at 300 atm), flywheels (∼0.5 MJ/kg), supercapacitors (∼0.01 MJ/kg), and pumped water (0.001 MJ/kg at 100 m) are modest. The same is true of batteries, which are often discussed as an effective energy storage medium for solar energy. Though considerable efforts are currently being devoted to battery development,[7] most advances have little

*To whom correspondence should be addressed. E-mail: nocera@mit.edu.

(1) Hoffert, M. I.; Caldeira, K.; Jain, A. K.; Haites, E. F.; Harvey, L. D. D.; Potter, S. D.; Schlesinger, M. E.; Schneider, S. H.; Watts, R. G.; Wigley, T. M. L.; Wuebbles, D. J. *Nature* **1998**, *395*, 881.
(2) Nocera, D. G. *Daedalus* **2006**, *135*, 112.
(3) Lewis, N. S.; Nocera, D. G. *Proc. Natl. Acad. Sci. U.S.A.* **2006**, *103*, 15729.
(4) Eisenberg, R.; Nocera, D. G. *Inorg. Chem.* **2005**, *44*, 6799.
(5) Nocera, D. G. *ChemSusChem* **2009**, *2*, 387.
(6) Nocera, D. G. *Chem. Soc. Rev.* **2009**, *38*, 13.
(7) Owens, B. B.; Smyrl, W. H.; Xu, J. J. *J. Power Sources* **1999**, *81−82*, 150.

Published on Web 09/23/2009

Daniel G. Nocera is the Henry Dreyfus Professor of Energy and Professor of Chemistry, Director of the Solar Revolutions Project, and Director of the Eni Solar Frontiers Center at MIT. He studies the chemistry of renewable energy. He has discovered a solar fuel process that captures many of the elements of photosynthesis outside the leaf. His recent efforts are devoted to bringing personalized, carbon-neutral energy to the poor and those of the nonlegacy world.

to do with the energy density, but rather they are concerned with the power density (i.e., the rate at which charge can flow in and out of the battery) and lifetime. Energy densities of batteries are low (~0.1−0.5 MJ/kg) with little room for improvement because the electron is stored at a metal center of an inorganic network juxtaposed to an electrolyte. The volume in which the electron and attendant cation reside and transfer is thus limited by the physical density of the materials. Some of the lightest elements in the periodic table, and hence lowest physical densities, are already used as battery materials, and consequently the energy densities of batteries have approached a ceiling. If we continue along this line of reasoning, the smallest-volume element in which electrons may be stored is in the chemical bond. It is for this reason that the energy density of liquid fuels (~50 MJ/kg) is $\geq 10^2$ times larger than the best of the foregoing storage methods; dihydrogen (H_2) possesses an even greater energy density at 140 MJ/kg. Indeed, society has intuitively understood this disparity in the energy density because all large-scale energy storage in our society is in the form of fuels.

HY (Y = halide or OH^-) splitting is a particularly attractive storage mechanism for solar PE:

$$2H_2O + \text{light} \rightarrow 2H_2 + O_2 \quad (1)$$

$$2HX + \text{light} \rightarrow H_2 + X_2 \quad (2)$$

If X = Cl, both hydrohalic acid and water splitting are of similar formal potential at standard conditions and, consequently, store approximately the same amount of energy for reactions of equal electron equivalency. To understand the storage capacity of HY splitting, consider eq 1 within the context of the average American home, which uses ~20 kW-h of electricity per day. Given that the heat of formation of water is 237 kJ/mol, then the storage of 20 kW-h can be achieved by splitting only 5.5 L of water per day. On this basis, a system such as that shown in Figure 1 can provide sufficient PE to support an individual's daily life. Of course, compression efficiencies for H_2 and the efficiency of the fuel cell must also be factored into the system, thus increasing the amount of water that needs to be split. The point here is that

Scheme 1

Water Splitting

$$2H_2O \longrightarrow 2H_2 + O_2$$

$$4H^+ + 4e^- \longrightarrow 2H_2$$

$$2H_2O \longrightarrow O_2 + 4e^-$$

HX Splitting

$$2HX \longrightarrow H_2 + X_2$$

$$2H^+ + 2e^- \longrightarrow H_2$$

$$2X^- \longrightarrow X_2 + 2e^-$$

energy storage needed for solar PE is currently within reach of the chemist with the design of catalysts that effectively promote eq 1 or 2 in the forward (solar storage) and reverse (fuel cell) directions.

Successful HY splitting at high efficiencies demands significant discovery on several fronts. Scheme 1 separates eqs 1 and 2 into their half-reactions. The overall transformation involves either 1 × 2e (for H_2) and 1 × 2e (for X_2) or 2 × 2e (for H_2) and 1 × 4e (for O_2) *multielectron* processes to which *protons* must be coupled intimately. If they are not, then prohibitively high-energy barriers are imposed on both half-reactions. Moreover, HY-splitting reactions confront sizable thermodynamic barriers that are intrinsic to the energy storage process. Whereas chemists have mastered catalytic reactions of energy-rich bonds in downhill reactions, the efficient catalytic bond-making/breaking reactions of *energy-poor substrates* are not generally realized at a molecular center or on a surface. This is especially pertinent to the HY-splitting problem because photointermediates invariably contain strong metal−X bonds, which need to be activated to close a catalytic cycle. In this context, a toolbox for HY splitting is as follows: (a) multielectron transformations, (b) rearrangement of low-energy bonds to high-energy bonds (i.e., running reactions uphill with an energy input), and (c) proton-coupled electron transfer (PCET). The HY-splitting problem shares basic chemical commonalities to the activation of other small molecules of energy consequence as well,[8,9] including CO_2, N_2, CH_4, H_2, and O_2. For this reason, (a)−(c) more generally underpin the molecular chemistry of renewable energy. Our research effort to systematically develop the chemistry of processes (a)−(c) is presented. With these "new colors" on the chemistry palette, a picture of solar PE emerges.

2. A Chemist's Toolbox for Catalysis of Consequence to Renewable Energy

2.1. Multielectron Chemistry. The endergonic nature of energy conversion chemistry demands an energy input

(8) Dempsey, J. L.; Esswein, A. J.; Manke, D. R.; Rosenthal, J.; Soper, J. D.; Nocera, D. G. *Inorg. Chem.* **2005**, *44*, 6879.

(9) Rosenthal, J.; Bachman, J.; Dempsey, J. L.; Esswein, A. J.; Gray, T. G.; Hodgkiss, J. M.; Manke, D. R.; Luckett, T. D.; Pistorio, B. J.; Veige, A. S.; Nocera, D. G. *Coord. Chem. Rev.* **2005**, *249*, 1316.

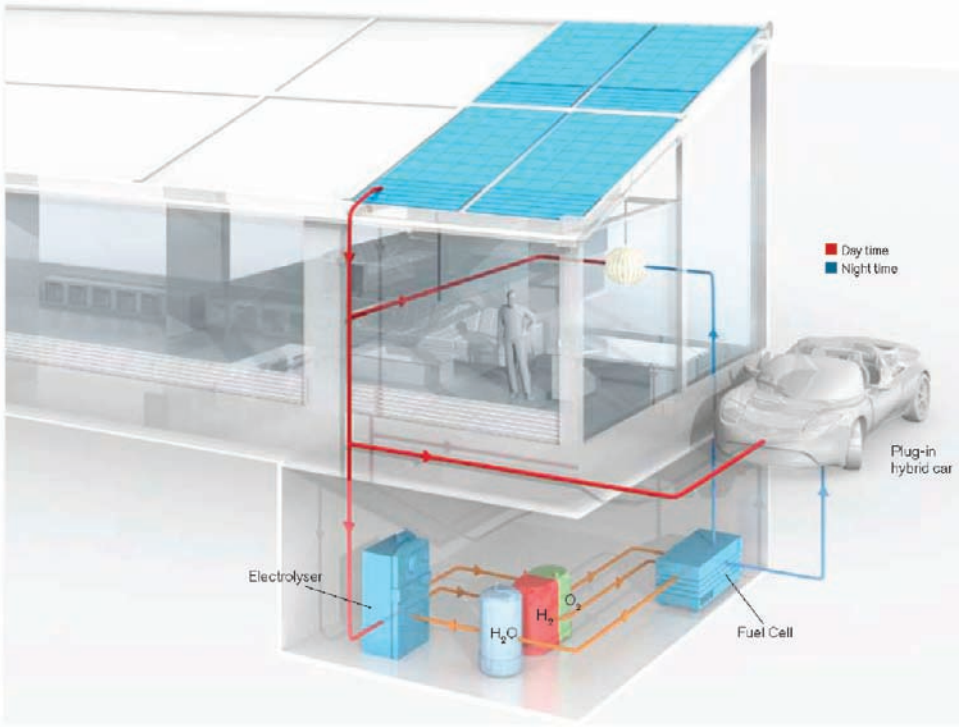

Figure 1. Energy-independent home delivering the individual PE. Reproduced with permission from MIT and Technology Review.

in order to drive the reaction. Often that energy input comes from light, which produces an electronic excited state from which the reaction proceeds. The oxidation−reduction reactions of electronically excited transition-metal complexes customarily proceed by one electron. Multielectron reactivity is achieved by coupling consecutive one-electron processes to a remote homogeneous or heterogeneous site, which is capable of storing multiple redox equivalents. This general strategy has largely defined the light-to-energy conversion schemes of the past 4 decades.[10−14] Such conformity in multielectron design finds its origins in the nature of the excited state (Figure 2), which at the most general level is the same despite the many different types of transition-metal photoreagents. The photochemistry of mononuclear d^6 metals, for which tris(bipyridyl)-ruthenium(II) is the archetype, originates from a metal-to-ligand charge-transfer (MLCT) excited state[15−19] in which electrons localized on the metal and ligand are triplet-paired. Biradical excited states are also obtained from binuclear complexes but in different guises. The $d\sigma-d\sigma^*$ (or $d\pi^*-d\sigma^*$) excited states of d^7-d^7 and d^9-d^9 complexes are short-lived and dissociative, producing a $^{\bullet}M/M^{\bullet}$ biradical pair.[20−22] Metal-based biradicals are tethered by a single bond upon production of a $d\sigma^*-p\sigma$ excited state of $d^8\cdots d^8$ and $d^{10}\cdots d^{10}$ complexes.[23,24] For each of the three types of excited states, the biradical naturally leads to two-electron processes, one electron at a time,[18,23,25] and a controlled multielectron chemistry is difficult to achieve.

2.1.1. Multielectron Excited State. To develop a discrete multielectron excited state, we returned to the most basic element of chemistry, the two-electron, two-center (2e−2c) bond. This electronic configuration gives rise to four states, which for H_2 are derived from the $^1\sigma\sigma$, $^3\sigma\sigma^*$, $^1\sigma\sigma^*$, and $^1\sigma^*\sigma^*$ configurations shown in Figure 3. The $^1\Sigma_u(^1\sigma\sigma^*)$ and $^3\Sigma_u(^3\sigma\sigma^*)$ excited states involve one-electron promotion and thus lie about the one-electron orbital splitting energy (ΔW), separated by twice the exchange energy (K). Because electrons reside in a molecular orbital (MO) that is well distributed about the two hydrogen atoms, the distance between the electrons, r_{ij}, is large and, hence, K is small. Consequently, the energies of $^1\Sigma_u(^1\sigma\sigma^*)$ and $^3\Sigma_u(^3\sigma\sigma^*)$ are well accounted for by

(10) Kalyanasundaram, K., Grätzel, M., Eds. Photosensitization and Photocatalysis Using Inorganic and Organometallic Compounds. *Catalysis by Metal Complexes*; Kluwer Academic: Dordrecht, The Netherlands, 1993; Vol. *14*, p 247.
(11) Balzani, V.; Barigelletti, F.; Decola, L. *Top. Curr. Chem.* **1990**, *158*, 31.
(12) Amouyal, E. In *Homogeneous Photocatalysis*; Chanon, M., Ed.; Wiley: New York, 1997; p 263.
(13) Sutin, N.; Creutz, C.; Fujita, E. *Comments Inorg. Chem. A* **1997**, *19*, 67.
(14) Bard, A. J.; Fox, M. A. *Acc. Chem. Res.* **1995**, *28*, 141.
(15) Schoonover, J. R.; Bignozzi, C. A.; Meyer, T. J. *Coord. Chem. Rev.* **1997**, *165*, 239.
(16) Krausz, E.; Ferguson, J. *Prog. Inorg. Chem.* **1989**, *37*, 293.
(17) Juris, A.; Balzani, V.; Barigelletti, F.; Campagna, S.; Belser, P.; von Zelewsky, A. *Coord. Chem. Rev.* **1988**, *84*, 85.
(18) Kalyanasundaram, K. *Photochemistry of Polypyridine and Porphyrin Complexes*; Academic Press: London, 1982; Chapter 6.
(19) Crosby, G. L. *Acc. Chem. Res.* **1975**, *8*, 231.
(20) Rothberg, L. J.; Cooper, N. J.; Peters, K. S.; Vaida, V. *J. Am. Chem. Soc.* **1982**, *104*, 3536.
(21) Zhang, J. Z.; Harris, C. B. *J. Chem. Phys.* **1991**, *95*, 4024.
(22) Kim, S. K.; Pedersen, S.; Zewail, A. H. *Chem. Phys. Lett.* **1995**, *233*, 500.
(23) Roundhill, D. M.; Gray, H. B.; Che, C.-M. *Acc. Chem. Res.* **1989**, *22*, 55.
(24) Fordyce, W. A.; Brummer, J. G.; Crosby, G. A. *J. Am. Chem. Soc.* **1981**, *103*, 7061.
(25) Geoffrey, G. L.; Wrighton, M. S. *Organometallic Photochemistry*; Academic Press: New York, 1979.

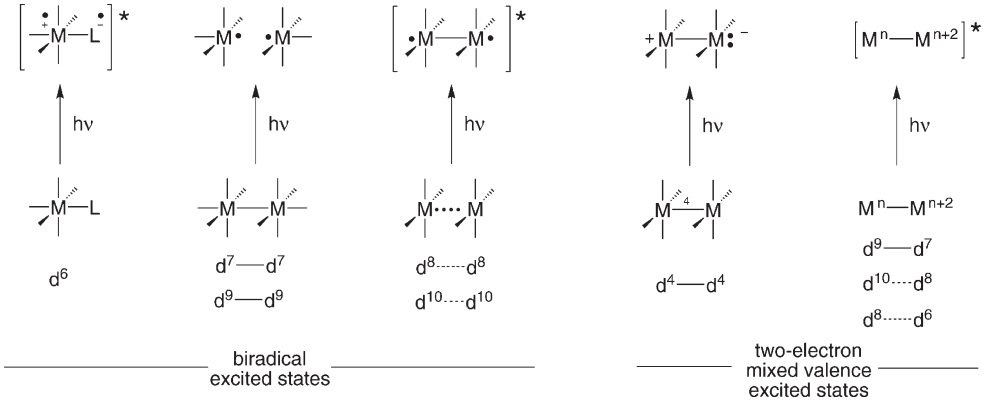

Figure 2. Electron configurations for the diradical excited state that is characteristic of most transition-metal complexes and the two-electron mixed-valence excited state of bimetallic compounds explored in the author's research program.

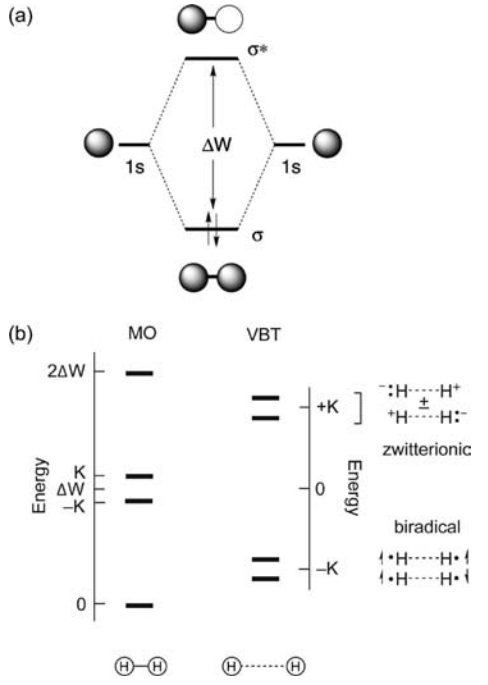

Figure 3. MO diagram of H_2 (top) and the energy level diagram for H_2 described in the limits of MOT and VBT (bottom). ΔW is the one-electron orbital splitting energy, and K is the two-electron exchange energy.

ΔW in the MO limit. The $2^1\Sigma_g(^1\sigma^*\sigma^*)$ excited state is derived from a two-electron promotion and, hence, it lies at $2\Delta W$.

The 2e−2c manifold holds a central place in bonding descriptions. It was originally described by Heitler and London for valence bond theory (VBT)[26] and subsequently by Pauling[27] and Mulliken[28] in their formalism of MO theory (MOT). Although the state diagram for strongly overlapping orbitals (i.e., the MO limit), such as the one shown in Figure 3, is taught at the most introductory level of chemistry, it is not generally appreciated when the orbitals are weakly coupled. Coulson and Fischer described this case for "stretched hydrogen" in their landmark paper that unified VBT and MOT.[29] At long distance, the 1s orbitals of H_2 overlap marginally. Two low-energy biradical states arise from one electron in each orbital, with spins opposed in the $^1\sigma\sigma$ ground state and parallel in the $^3\Sigma_u(^3\sigma\sigma^*)$ excited state. Because the orbitals are weakly overlapping, ΔW is small and these states are of similar energy. Of pertinence to multielectron chemistry, the two higher-energy $^1\Sigma_u(^1\sigma\sigma^*)$ and $2^1\Sigma_g(^1\sigma^*\sigma^*)$ configurations correlate to zwitterionic singlet excited states that are derived from the antisymmetric and symmetric linear combinations of electrons paired in one orbital of either center. The high energy of the zwitterionic states ($2K$ above the ground state) results from the sizable exchange energy that is incurred upon the pairing of two electrons in atomic-like orbitals. Unlike the biradical state, this type of zwitterionic excited state is predisposed to two-electron reactivity.

The four states of the 2e−2c bond had not been directly measured experimentally prior to our work. The reason is simple: The excited states of the four-electron manifold are antibonding and thus dissociative. This challenge is especially acute for the highest-energy singlet state, which amounts to the promotion of two electrons into an antibonding orbital. It is difficult to stretch a σ bond or twist a π bond and maintain a stable configuration for spectroscopic delineation of the energetics of that bond.[30] Conversely, the overlap of the d_{xy} orbitals on individual metal centers presents a stable 2e−2c δ bond, which is ideally adapted for spectroscopic investigation when incorporated within the sterically constrained coordination environment of quadruple metal−metal-bonded species (M−4−M).[31] In this case, the four states in D_{4h} symmetry resulting from the electron occupation of the δ highest occupied MO (HOMO) and δ^* lowest unoccupied MO (LUMO) are $^1A_{1g}(^1\delta\delta)$, $^3A_{2u}(^3\delta\delta^*)$, $^1A_{2u}(^1\delta\delta^*)$, and $2^1A_{1g}(^1\delta^*\delta^*)$, each of which has been independently characterized.

With the formulation of the δ bond,[32,33] the identification of the $^1A_{1g}(^1\delta\delta)$ ground state in M−4−M species

(26) Heitler, W.; London, F. *Z. Phys.* **1927**, *44*, 455.
(27) Pauling, L. *Chem. Rev.* **1928**, *5*, 173.
(28) Mulliken, R. S. *Phys. Rev.* **1928**, *32*, 186.
(29) Coulson, C. A.; Fischer, I. *Philos. Mag.* **1949**, *40*, 386.
(30) Even here, inorganic chemistry has made the unimaginable a reality. A "stretched" π bond has been isolated in a stabilized configuration by using a Hg^{2+} ion to juxtapose two Mo(silox)$_2$N^{t}Bu cores at long distance. See: Rosenfeld, D. C.; Wolczanski, P. T.; Barakat, K. A.; Buda, C.; Cundari, T. R. *J. Am. Chem. Soc.* **2005**, *127*, 8262.
(31) Cotton, F. A.; Nocera, D. G. *Acc. Chem. Res.* **2000**, *33*, 483.
(32) Figgis, B. M.; Martin, R. L. *J. Chem. Soc.* **1956**, 3837.
(33) Ross, I. G. *Trans. Faraday Soc.* **1959**, *55*, 1057.

soon followed.[34] The strong polarization and dipole allowedness of the $\delta \rightarrow \delta^*$ transition led to the identification of the $^1A_{2u}(^1\delta\delta^*)$ excited state early in the study of the electronic absorption spectroscopy of these compounds.[35] The $^3A_{2u}(^3\delta\delta^*)$ state is sufficiently low in energy, as first predicted by Hay,[36] that it can be populated at reasonable temperatures, thus allowing its energy to be determined from temperature-dependent measurements of the magnetic susceptibility[37] and of ligand $^{31}P\{^1H\}$ NMR signals.[38] Against this backdrop, we sought to observe the $2^1A_{1g}(^1\delta^*\delta^*)$ excited state. We located the $2^1A_{1g}(^1\delta^*\delta^*)$ excited state, which is two-electron excitation forbidden by the selection rules of conventional optical spectroscopy, by two-photon laser-induced fluorescence (TP-LIF).[39,40] The TP-LIF experiment is schematically represented in Figure 4. The $2^1A_{1g}(^1\delta^*\delta^*)$ state is accessed with two near-IR photons, followed by internal conversion to the emissive $^1A_{2u}(^1\delta\delta^*)$ excited state. The $2^1A_{1g}(^1\delta^*\delta^*)$ excitation profile is constructed by monitoring the intensity of the $^1A_{2u}(^1\delta\delta^*)$ luminescence as the IR excitation wavelength (normalized in intensity) is scanned in and out of resonance with the $2^1A_{1g}(^1\delta^*\delta^*)$ state. The assignment of the two-photon state follows from power-dependent measurements and polarization ratios over the entire two-photon absorption cross section. This result, together with the previous spectroscopic measurements of the $^3A_{2u}(^1\delta\delta^*)$ and $^1A_{2u}(^1\delta\delta^*)$ excited states, provided the first complete description of the four states that characterize a 2e−2c bond in a discrete molecular species.[31]

The overall wavefunction is defined by ΔW, K, and the overlap integral, S, of the two d_{xy} orbitals.[41] With three state energies on hand, these three spectroscopic unknowns may be unambiguously calculated and the coefficients, and hence the degree of ionicity, of the excited-state wavefunctions may be determined.[31,39] Our results on $M_2X_4(PP)$ ($M = Mo^{II}, W^{II}$; X = halide; PP = bridging phosphine) reveal that the $^1\delta\delta$ ground state possesses 20% ionic character, which increases to 80% in the $^1A_{2u}(^1\delta\delta^*)$ excited state. These two-photon results unequivocally establish the significant zwitterionic character of the $^1A_{2u}(^1\delta\delta^*)$ excited state:

$$\Psi(^1\delta\delta^*) = {}^-\!:\!M-^3-M^+[d^5-d^3] - M^+-^3-M:^-[d^3-d^5] \quad (3)$$

The zwitterionic $^1A_{2u}(^1\delta\delta^*)$ excited state is of sufficient lifetime to permit excited-state reactivity, though we found that this is not a sufficient condition for multielectron photochemistry. Although the $^1A_{2u}(^1\delta\delta^*)$ excited state is ionic, it is nonpolar because

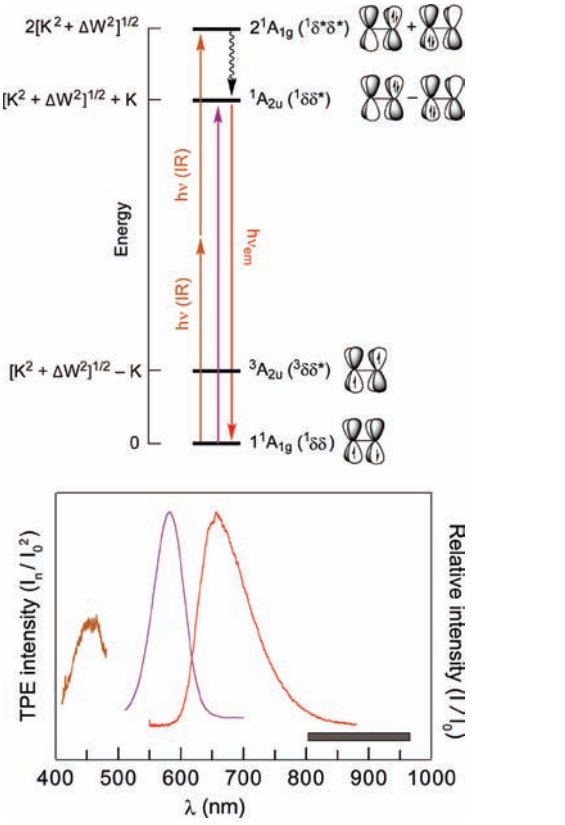

Figure 4. (Top) Qualitative energy level diagram for the δ/δ^* orbital manifold arising from the overlap of d_{xy} orbitals of M−4−M complexes in accordance with a valence bond model. The $^1\delta^*\delta^*$ excited state can be accessed by two-photon near-IR absorption and detected via LIF of the $^1\delta\delta^*$ excited state. The energy of the states is given in terms of the one-electron orbital splitting energy ΔW and the two-electron exchange energy K. (Bottom) Emission (red), absorption (purple), and TP-LIF excitation (brown) spectra of $Mo_2Cl_4(PMe_3)_4$ in 3-methylpentane at room temperature. The TP-LIF excitation spectrum is superimposed at twice the laser excitation energy. The spectral region over which the incident dye-laser excitation was scanned is indicated by the gray box.

$^-$:M−3−M$^+$ and $^+$M−3−M:$^-$ are equal contributors to the linear combination of eq 3 as long as a center of inversion is maintained within the molecule and its environment. Intermolecular or intramolecular perturbations are needed to remove the center of inversion and, consequently, engender an electronic asymmetry. Transient spectroscopy of M−4−M complexes reveal that the two-electron mixed-valence character of the zwitterionic excited state is trapped by an intramolecular ligand rearrangement to yield an edge-sharing bioctahedral (ESBO) intermediate with two electrons localized on one metal center of the bimetallic core.[42]

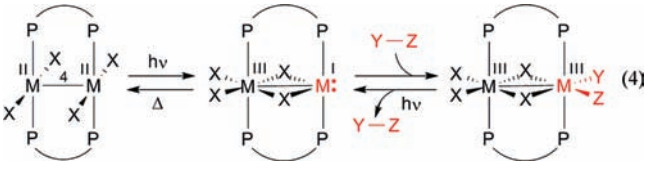

The resultant $^+$M−3−M:$^-$ zwitterion reacts in discrete two-electron steps: $M_2X_4(PP)_2$ ($M = Mo^{II}, W^{II}$; X = halide;

(34) Cotton, F. A.; Curtis, N. F.; Harris, C. B.; Johnson, B. F. G.; Lippard, S. J.; Mague, J. T.; Robinson, W. R.; Wood, J. S. *Science* **1964**, *145*, 1305.
(35) Cowman, C. D.; Gray, H. B. *J. Am. Chem. Soc.* **1973**, *95*, 8177.
(36) Hay, P. J. *J. Am. Chem. Soc.* **1982**, *104*, 7007.
(37) Hopkins, M. D.; Zietlow, T. C.; Miskowski, V. M.; Gray, H. B. *J. Am. Chem. Soc.* **1985**, *107*, 510.
(38) Cotton, F. A.; Eglin, J. L.; Hong, B.; James, C. A. *J. Am. Chem. Soc.* **1992**, *114*, 4915.
(39) Engebretson, D. S.; Zaleski, J. M.; Leroi, G. E.; Nocera, D. G. *Science* **1994**, *265*, 759.
(40) Engebretson, D. S.; Graj, E. M.; Leroi, G. E.; Nocera, D. G. *J. Am. Chem. Soc.* **1999**, *121*, 868.
(41) Hopkins, M. D.; Gray, H. B.; Miskowski, V. M. *Polyhedron* **1987**, *6*, 705.
(42) Hsu, T. L. C.; Helvoigt, S. A.; Partigianoni, C. M.; Turró, C.; Nocera, D. G. *Inorg. Chem.* **1995**, *34*, 6186.

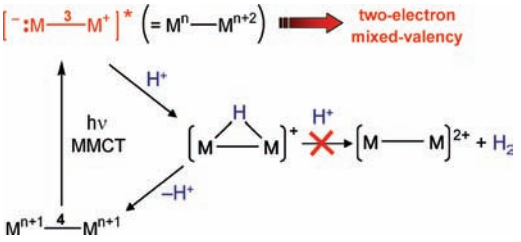

Figure 5. MMCT produces a zwitterionic excited state in which the formal oxidation states of the metal differ by two. Transient absorption studies show that the excited state reacts with a proton to make a hydride, which back-reacts to produce the M−4−M ground state. The hydride is not trapped by a second proton to produce hydrogen.

PP = bridging phosphine) complexes undergo one-photon two-electron addition of YZ substrates such as alkyl iodides[43,44] and aryl disulfides[42] to yield $M_2^{III,III}$ ESBO complexes. The same zwitterionic intermediate supports two-electron elimination reactions of isovalent ESBO complexes (the photodriven reverse of eq 4).[45] Whereas the two-electron zwitterionic intermediate may be trapped by a proton as well (see Figure 5), the ensuing species is not hydridic enough to be protonated to produce hydrogen.

2.1.2. Two-Electron Mixed Valency. The two-electron reaction intermediate of M−4−M complexes is produced by light excitation of a metal-to-metal charge-transfer transition. This two-electron character resulting from electron pairing within the binuclear core of M−4−M species is quite unique. Most excited states are derived from the population of MOs that are delocalized over the entire bimetallic core and, consequently, it is inappropriate to think about electron-pair localization at one metal or another. For this reason, multielectron schemes based on zwitterionic excited states are difficult to generalize and new approaches to multielectron reactivity must be developed. To this end, we set a research course to incorporate two-electron mixed valency into the delocalized ground state of bimetallic complexes.

2.1.2.1. Metal-Based Two-Electron Mixed-Valence Complexes. The zwitterionic excited state may be formulated as a two-electron mixed-valence species, as depicted in Figure 5. This formalism is useful because it provides connectivity to a large body of inorganic chemistry that was pioneered by Taube.[46] Mixed valency in molecular compounds is typically accommodated at metal centers whose formal oxidation states differ by one.[47−49] In these complexes, reactivity is confined to *single*-electron

Scheme 2

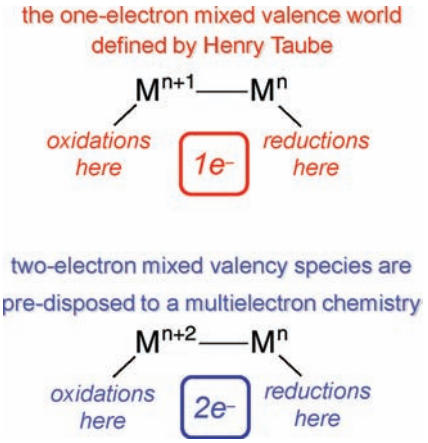

oxidations and reductions of the constituent M^n and M^{n+1} centers, respectively.[50−55] Extrapolating from this one-electron formalism, two-electron mixed valency of bimetallic cores provides entry into *multi*electron oxidation−reduction chemistry (Scheme 2).[56] Redox cooperativity may be established between the individual metal centers of a $M^n\cdots M^{n+2}$ mixed-valence core such that two-electron oxidations may be promoted at a M^{n+2} center and two-electron reductions may be promoted at a M^n center.

A metal-based two-electron mixed valency in a delocalized electronic ground state is attained by the disproportionation of a redox symmetric core,

$$M^{n+1}-M^{n+1} \rightleftharpoons M^n-M^{n+2} \quad (5)$$

Equation 5 may be driven to the right by designing ligands that incorporate antithetical design elements: two π-accepting moieties with a π-donor bridgehead (A−D−A)[57−61] or two π-donating moieties with a π-accepting bridgehead (D−A−D).[62−64] The A−D−A ligand motif is achieved by placing an amine bridgehead between two electron-deficient phosphines (PR^F_2) or phosphites ($P(OR^F)_2$). The A−D−A ligands bis(difluorophosphino)methylamine (dfpma, $CH_3N(PF_2)_2$) and bis-[bis(trifluoroethoxy)phosphino]methylamine (tfepma, $CH_3N[P(OCH_2CF_3)_2]_2$), shown in Chart 1, exhibit a

(43) Partigianoni, C. M.; Turró, C.; Hsu, T. L. C.; Chang I.-J.; Nocera, D. G. *Photosensitive Metal-Organic Systems; Mechanistic Principles and Applications*; Advances in Chemistry Series 238; Kutal, C., Serpone, N., Eds; American Chemical Society: Washington, DC, 1993; p 147.
(44) Partigianoni, C. M.; Nocera, D. G. *Inorg. Chem.* **1990**, *29*, 2033.
(45) Pistorio, B. J.; Nocera, D. G. *Chem. Commun.* **1999**, 1831.
(46) Taube, H. *Angew. Chem., Int. Ed. Engl.* **1984**, *23*, 329.
(47) Creutz, C. *Prog. Inorg. Chem.* **1983**, *30*, 1.
(48) *Mixed Valency System: Applications in Chemistry, Physics and Biology*; Prassides, K., Ed.; NATO ASI Series C: Mathematical and Physical Sciences 343; Kluwer Academic: Dordrecht, The Netherlands, 1991.
(49) Schatz, P. N. In *Inorganic Electronic Structure and Spectroscopy*; Solomon, E. I., Lever, A. B. P., Eds.; Wiley-Interscience: New York, 1999; Vol. *2*, p 175.
(50) Ito, T.; Hamaguchi, T.; Nagino, H.; Yamaguchi, T.; Kido, H.; Zavarine, I. S.; Richmond, T.; Washington, J.; Kubiak, C. P. *J. Am. Chem. Soc.* **1999**, *121*, 4625.
(51) Ito, T.; Hamaguchi, T.; Nagino, H.; Yamaguchi, T.; Washington, J.; Kubiak, C. P. *Science* **1997**, *277*, 660.
(52) Vahrenkamp, H.; Geiss, A.; Richardson, G. N. *J. Chem. Soc., Dalton Trans.* **1997**, 3643.
(53) Balzani, V.; Juris, A.; Venturi, M.; Campagna, S.; Serroni, S. *Chem. Rev.* **1996**, *96*, 759.
(54) Kunkely, H.; Pawlowski, V.; Vogler, A. *Inorg. Chim. Acta* **1994**, *225*, 327.
(55) Vogler, A.; Osman, A. H.; Kunkely, H. *Coord. Chem. Rev.* **1985**, *64*, 159.
(56) Nocera, D. G. *Acc. Chem. Res.* **1995**, *28*, 209.
(57) Heyduk, A. F.; Macintosh, A. M.; Nocera, D. G. *J. Am. Chem. Soc.* **1999**, *121*, 5023.
(58) Odom, A. L.; Heyduk, A. F.; Nocera, D. G. *Inorg. Chim. Acta* **2000**, *297*, 330.
(59) Heyduk, A. F.; Nocera, D. G. *J. Am. Chem. Soc.* **2000**, *122*, 9415.
(60) Heyduk, A. F.; Nocera, D. G. *Chem. Commun.* **1999**, 1519.
(61) Veige, A. S.; Nocera, D. G. *Chem. Commun.* **2004**, 1958.
(62) Manke, D. R.; Loh, Z.-H.; Nocera, D. G. *Inorg. Chem.* **2004**, *43*, 3618.
(63) Manke, D. R.; Nocera, D. G. *Inorg. Chem.* **2003**, *42*, 4431.
(64) Manke, D. R.; Nocera, D. G. *Inorg. Chim. Acta* **2003**, *345*, 235.

particular proclivity for promoting the internal disproportionation of binuclear $M_2^{I,I}$ cores to $M_2^{0,II}$ cores[65] for the metals of rhodium[57,58] and iridium.[59−61,66] X-ray crystal structures reveal a pronounced asymmetry in the diphosphazane framework upon ligation to a bimetallic core derived from the asymmetric stabilization of metals that differ by 2 in their formal oxidation. The result is consistent with π donation of the amine bridgehead lone pair to the PR^F_2 bonded to M^{II}. With $M^{II} \rightarrow PR^F_2$ π-back-bonding diminished, the PR^F_2 group acts more like a simple σ donor, stabilizing the high-valent M^{II} metal center. Correspondingly, with the nitrogen lone-pair electron density channeled away from the second neighboring PR^F_2 group, its strong π-accepting properties are maintained, and hence M^0 is stabilized. As highlighted by the arrows in Figure 6, this electronic asymmetry is reflected in an alternating bond-length pattern for the $Rh^0-P-N-P-Rh^{II}$ framework.

Our success in using $M^n\cdots M^{n+2}$ species to drive two- and four-electron transformations along ground- and excited-state pathways[57−59] established two-electron mixed valency as a useful design concept for the development of multielectron reaction schemes. The two-electron mixed-valence core is particularly effective in hydrogen management and production.[67,68] Intermetal redox cooperation for hydrogen atom migration appears to be a critical determinant for the addition and elimination of hydrogen from $M^n\cdots M^{n+2}$ cores. The migration proceeds through a bridging hydride transition state,

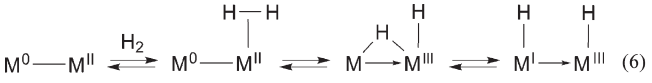

(6)

The ability of the diphosphazane ligand framework to accommodate the electronic and steric asymmetry without excessive reorganization as the hydrogen migrates among terminal and bridging coordination sites appears to be essential for the H_2 reactivity of eq 6.

The bridging transition state of eq 6 is similar to that proposed for the so-called dinuclear elimination mechanism for the bimolecular reductive elimination reaction of mononuclear species.[69−71] Some metal hydrides, which exhibit sluggish intramolecular elimination, are extremely unstable in the presence of a second complex capable of attaining coordinative unsaturation. This enhanced reactivity has been ascribed to the following transformation,

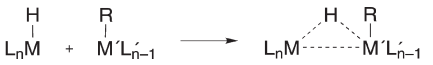

(7)

in which R is a hydride, alkyl, or acyl group. Bimolecular elimination of this type is only possible when one of the ligands is a hydride, which must migrate to the bridging position for elimination to occur. For the case of the two-electron mixed-valence compounds, the requisite coordinative unsaturation and hydride are already present. With the neighboring metals of the $M^n\cdots M^{n+2}$ core working in concert, the hydrogen atom migrates to and from the critical bridging position to promote facile H_2 addition and elimination,[67] respectively. In this regard, we view the chemistry of the two-electron mixed-valence complexes as the unimolecular analogue to the dinuclear elimination reaction.

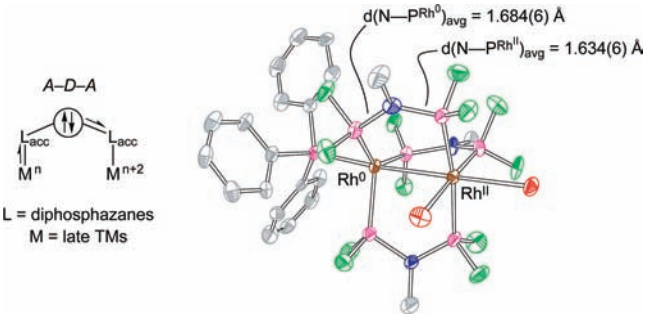

Figure 6. (Left) Three-atom dfpma ligand shown in Chart 1 possessing an electron-donor bridgehead (D) between two π-accepting moieties (A), which can be used to stabilize two-electron mixed-valence cores. The stabilization of a mixed-valence core by the A−D−A stereoelectronic ligand motif results in differing bond orders indicative of an asymmetric electronic distribution. (Right) Crystal structure of $Rh_2^{0,II}(dfpma)_3Br_2$ displaying the long−short bond alteration of the ligand backbone. Reproduced from ref 8.

Chart 1. Fluorophosphine Ligands that Promote Two-Electron Mixed Valency of Bimetallic Cores

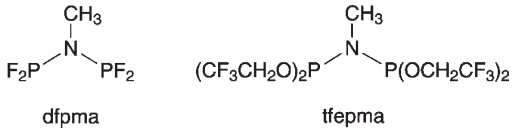

2.1.2.2. Ligand-Based Two-Electron Mixed-Valence Complexes. The design concept of two-electron mixed valency is expanded by using the ligand framework of porphyrinogens as the multielectron/hole reservoir, as opposed to the bimetallic core. Oxidation of the tetrapyrrole ring of porphyrinogen results in one or two spirocyclopropane rings (Δ), formed by C−C coupling between the α carbon atoms of neighboring pyrroles.[72] This transformation effectively stores two or four oxidizing equivalents in the macrocyclic ring. Prior to our studies, however, the generality, characterization, and practical use of the ligand-based redox chemistry of porphyrinogens was hindered by the presence of redox-active axial ligands and/or polynuclear copper/iron halide counterions.[73−75] Accordingly, we developed new synthetic methods that afforded porphyrinogens with

(65) Gray, T. G.; Nocera, D. G. *Chem. Commun.* **2005**, 1540.
(66) Esswein, A. J.; Veige, A. S.; Nocera, D. G. *Organometallics* **2008**, *27*, 1073.
(67) Veige, A. S.; Gray, T. G.; Nocera, D. G. *Inorg. Chem.* **2005**, *44*, 17.
(68) Gray, T. G.; Veige, A. S.; Nocera, D. G. *J. Am. Chem. Soc.* **2004**, *126*, 9760.
(69) Norton, J. R. *Acc. Chem. Res.* **1979**, *12*, 139.
(70) Martin, B. D.; Warner, K. E.; Norton, J. E. *J. Am. Chem. Soc.* **1986**, *108*, 33.
(71) Kristjánsdóttir, S. S.; Norton, J. A. In *Transition Metal Hydrides*; Dedieu, A., Ed.; VCH: New York, 1992; Chapter 9, p 309.
(72) Floriani, C.; Floriani-Moro, R. In *The Porphyrin Handbook*; Kadish, K., Smith, K. M.; Guilard, R., Eds.; Academic Press: San Diego, CA, 2000; Vol. *3*, Chapter 25, p 405.
(73) De Angelis, S.; Solari, E.; Floriani, C.; Chiesi-Villa, A.; Rizzoli, C. *J. Am. Chem. Soc.* **1994**, *116*, 5691.
(74) De Angelis, S.; Solari, E.; Floriani, C.; Chies-Villa, A.; Rizzoli, C. *J. Am. Chem. Soc.* **1994**, *116*, 5702.
(75) Crescenzi, R.; Solari, E.; Floriani, C.; Chiesi-Villa, A.; Rizzoli, C. *J. Am. Chem. Soc.* **1999**, *121*, 1695.

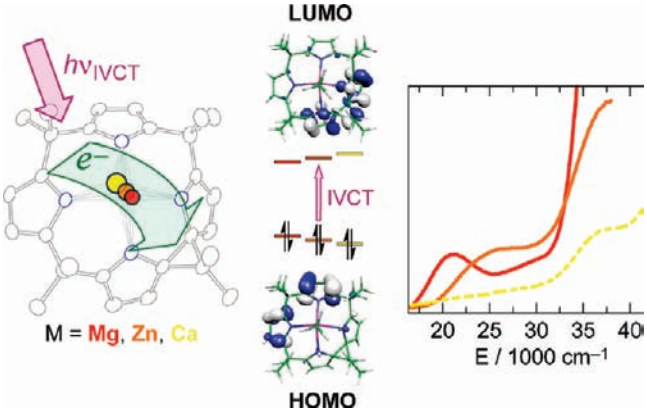

Figure 7. (Left) Thermal ellipsoid plot (50% probability level) for the solid-state structure of the two-electron mixed-valence magnesium porphyrinogen compound, $[L^{\Delta}Mg(NCMe)]\cdot CH_2Cl_2$. (Middle) Computed frontier Kohn−Sham orbital diagram of the HOMOs and LUMOs of $[L^{\Delta}Mg(NCMe)]$ showing the localization of the electron density that gives rise to the IVCT transition. (Right) UV−visible absorption spectra of $[L^{\Delta}Mg]$ (—, red), $[L^{\Delta}Zn]$ (− −, orange), and $[L^{\Delta}Ca]$ (---, yellow) in CH_2Cl_2. Reproduced from ref 76.

redox-inactive metals (e.g., magnesium, zinc, and calcium) and redox-inert and spectroscopically silent counterions.[76] In this way, we were able to unveil the redox properties of the macrocycle by electrochemistry and isolate and characterize the three ligand oxidation states, $[LM]^{2-}$, $[L^{\Delta}M]$, and $[L^{\Delta\Delta}M]^{2+}$.[77] Figure 7 summarizes the results from structural, computational, and spectroscopic results of the intermediate oxidation state, $[L^{\Delta}M]$, which is best described as a localized two-electron mixed-valence complex. Density functional theory calculations reveal that the HOMOs are localized on the reduced half of the macrocycle whereas the LUMOs are localized on the oxidized half of the porphyrinogen (Figure 7, middle). Consistent with this formulation, the intense orange color of $[L^{\Delta}M]$ arises from an intraligand intervalence charge transfer (IL-IVCT) from the reduced dipyrrole half of the macrocycle to its two-electron-oxidized dipyrrole neighbor.

Figure 8 highlights the parallel between ligand- and metal-based two-electron mixed valency. For both cases, the two-electron mixed-valence intermediate (1) is the linchpin that couples the two-electron chemistry of the individual redox centers (dipyrroles in the case of porphyrinogen and rhodium centers in the case of the bimetallic complex), (2) is the structural composite of the symmetrically oxidized and reduced congeners, and (3) has lowest-energy electronic transitions that are confined to the two-electron mixed-valence core. The ligand-based approach, however, differs from that of the metal-based approach in one important aspect. Because coordination geometry is inextricably linked to the metal oxidation state, two-electron/hole storage in the metal-based approach must be accompanied by alterations of the primary coordination sphere. Conversely, for the porphyrinogens, two-electron/hole storage occurs in the macrocycle periphery, decoupled from the acid−base chemistry of the metal. This orthogonalization between the redox storage and metal coordination geometry offers a new design element for using two-electron mixed valency to promote multielectron reactivity. This chemistry is contingent on relaying redox equivalents from the macrocycle to a redox-active central metal. We have demonstrated redox communication between the metal and ligand of iron porphyrinogens[78] in which redox cycling between the iron and the porphyrinogen ring occurs in a single three-electron redox step between $[LFe^{III}]^-$ and $[L^{\Delta\Delta}Fe^{II}]^{2+}$ species.[79] In conjunction with this multielectron relay chemistry, protons may coordinate at the α-pyrrole carbon,[80] which is the same site that is involved in two-electron redox storage. Hence, the proton and electron redox equivalents are collected at the same site. The coupling of the electron and proton suggests that porphyrinogens may permit hydrogen to be generated at the porphyrinogen periphery.

2.2. Rearrangement of Low-to-High Energy Bonds. When low-energy metal−ligand bonds can be activated, photocatalytic hydrogen cycles involving two-electron mixed-valence complexes may be realized. For the dirhodium dfpma complex described in section 2.1.2.1, the metal−halide bonds of the two-electron mixed-valence intermediate, $Rh^0-Rh^{II}(X)_2$, must be surmounted for H_2 photocatalysis to be achieved.[81] The photocatalytic hydrogen generation cycle shown in Figure 9 has been constructed for the dirhodium dfpma complex in a homogeneous solution.[82] Relevant intermediates of the photocycle have been identified based on the isolation and crystallization of dfpma, tfepma, and tfepm [bis(bis(trifluoroethoxy)phosphino]methane, $H_2C[P(OCH_2CF_3)_2]_2$) dirhodium analogues.[83] Circling clockwise about the photocycle shown in Figure 9, the HX addition product to the $Rh_2^{0,0}$ core has been isolated by H_2 addition to the $Rh_2^{0,II}$ dihalide tfepma complex. Photolysis of this $Rh_2^{II,II}$ dihydride−dihalide complex drives the prompt photoelimination of 1 equiv of H_2 to generate a blue $(X)Rh^I\cdots Rh^I(X)$ intermediate, which may be crystallized when the bimetallic core is coordinated by tfepm. The hydrogen elimination is quantitative and efficient, by virtue of the gaseous state of the photoproduct. The valence-symmetric, primary $(X)Rh^I\cdots Rh^I(X)$ photoproduct is unstable with respect to internal disproportionation to the $Rh^0-Rh^{II}(X)_2$ core. The disproportionation proceeds by folding a terminal halide into the bridging position of the bimetallic core; this intermediate may be isolated for a diiridium center ligated by tfepm. Photoexcitation of the $Rh^0-Rh^{II}(X)_2$ complex leads to trap-assisted halogen elimination and regeneration of the $Rh_2^{0,0}$ complex for reentry into the photocycle.

The overall photoefficiency for H_2 production by the $Rh_2^{0,0}$ dfpma catalyst is ~1%. This photoefficiency is the same as that measured independently for the photoconversion of $Rh_2^{0,II}(dfpma)_3Cl_2L$ to $Rh_2^{0,0}(dfpma)_3L_2$ ($\Phi_p = 7 \times 10^{-3}$).[57] These observations suggested to us

(76) Bachmann, J.; Nocera, D. G. *Inorg. Chem.* **2005**, *44*, 6930.
(77) Bachmann, J.; Nocera, D. G. *J. Am. Chem. Soc.* **2004**, *126*, 2829.
(78) Bachmann, J.; Nocera, D. G. *J. Am. Chem. Soc.* **2005**, *127*, 4730.
(79) Bachmann, J.; Hodgkiss, J. M.; Young, E. R.; Nocera, D. G. *Inorg. Chem.* **2007**, *46*, 607.
(80) Bachmann, J.; Teets, T. S.; Nocera, D. G. *Dalton Trans.* **2008**, 4549.
(81) Esswein, A. J.; Nocera, D. G. *Chem. Rev.* **2007**, *107*, 4022.
(82) Heyduk, A. F.; Nocera, D. G. *Science* **2001**, *293*, 1639.
(83) Esswein, A. J.; Veige, A. S.; Nocera, D. G. *J. Am. Chem. Soc.* **2005**, *127*, 16641.

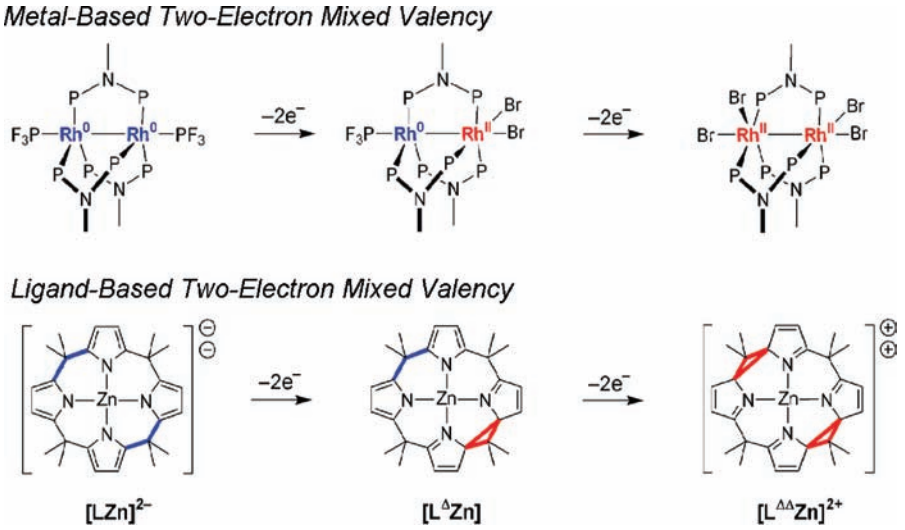

Figure 8. Porphyrinogen ligand as a two-electron mixed-valence scaffold and its redox parallel to the dirhodium system. The two-electron-reduced and -oxidized parts of the molecules are color-coded blue and red, respectively.

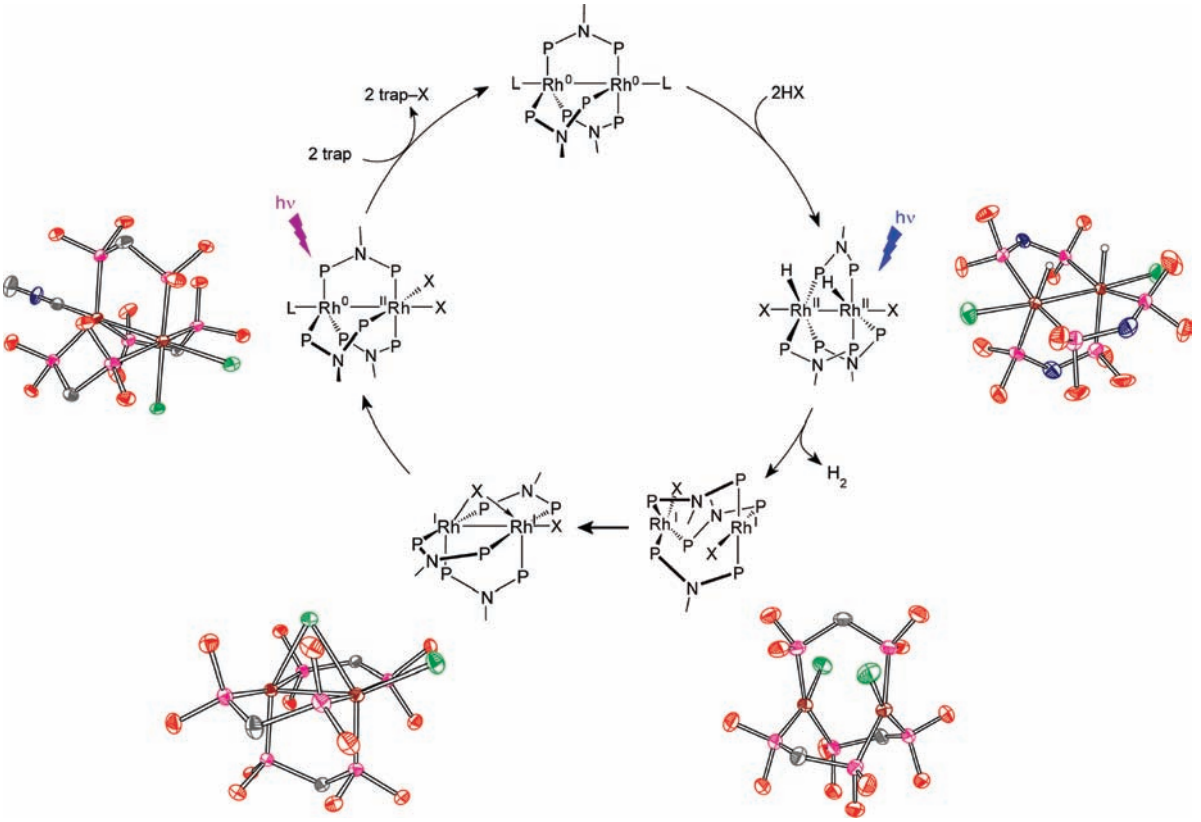

Figure 9. Complete photocycle for H_2 generation by the Rh_2 dfpma photocatalyst from nonaqueous solutions containing HCl or HBr. Identification of the intermediates in the cycle is based on the chemistry of dirhodium and diiridium dfpma, tfepma, and tfepm analogues, the crystal structures of which are shown.

that the activation of the Rh−X bond is determinant to the overall photocatalytic activity. An increase in the quantum efficiency for hydrogen photocatalysis is therefore equated to increasing the photoefficiency for halogen elimination from the binuclear metal core. The reductive elimination of dihalogen, however, is extremely rare because of the stability of the metal−halide bond together with the low bond energy of the halogen product. Moreover, the production of dihalogen is invariably endergonic. Even if dihalogen elimination is achieved, the back-reaction is thermodynamically favored and fast, resulting in no net reaction. For these reasons, the reductive elimination of halogen from metal centers proceeds only in the presence of a halogen trap.

Traps are problematic in that the trap−X bond is sufficiently exergonic that energy storage is obviated. In

addition, the detailed process by which photoelimination proceeds is obscured because both $X^{\bullet}$ and X_2 can react with most traps. Improved efficiencies for H_2 production therefore require increased quantum yields for M−X bond activation and new strategies to prevent the back-reaction of primary photoproducts.

We have succeeded in surmounting both challenges by incorporating gold and platinum into bimetallic cores.[84] The $[Pt^{III}Au^{II}(dppm)_2PhCl_3]PF_6$ [dppm = bis(diphenylphosphino)methane] complex photoreduces to its $Pt^{II}Au^{I}$ congener upon irradiation in the presence of 2,3-dimethyl-1,3-butadiene with a maximal quantum yield of 5.7%,[85] which is nearly a 10-fold increase over halogen elimination from the $Rh^0-Rh^{II}(X)_2$ bimetallic core. Even higher quantum yields are obtained from more highly oxidizing $Pt^{III}-Pt^{III}$ cores. $Pt_2^{III,III}(tfepma)_2Cl_6$ undergoes efficient two-electron photoreduction (Φ = 38%) to $Pt_2^{III,I}(tfepma)_2Cl_4$ under irradiation of λ_{exc} = 355−510 nm at high trap concentrations:[86]

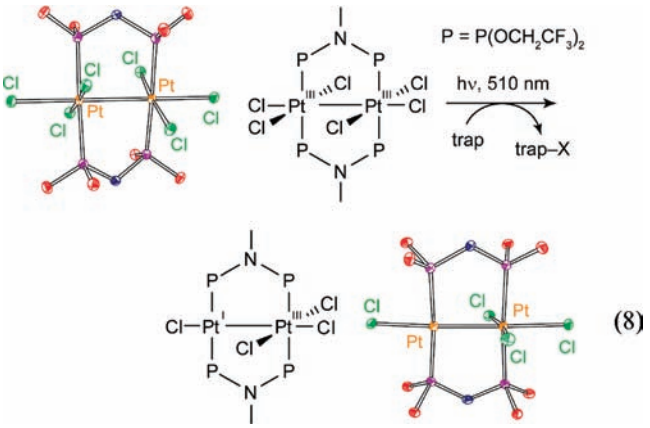

(8)

Because of the high quantum yield for halogen photoelimination, the reaction can be induced in the solid state in the absence of a trap. The experiment shown in Figure 10 provides the first example of authentic, trap-free X_2 reductive photoelimination from a transition-metal center. Of perhaps greater significance, Cl_2 adds facilely to the $Pt_2^{I,III}$ tfepma photoproduct. The photoreaction therefore is an authentic energy-storing photoreaction. The uphill photoreaction has been generalized to include Au^{III} centers of mono- and bimetallic cores coordinated by phosphines and bisphosphines, respectively.[87] In contrast to diplatinum photochemistry, which is driven from an excited state of considerable dσ^* parentage,[88] the digold chemistry appears to be derived from a ligand-to-metal charge-transfer (LMCT) excited state. Though LMCT photochemistry has been conventionally confined to one-electron redox transfor-

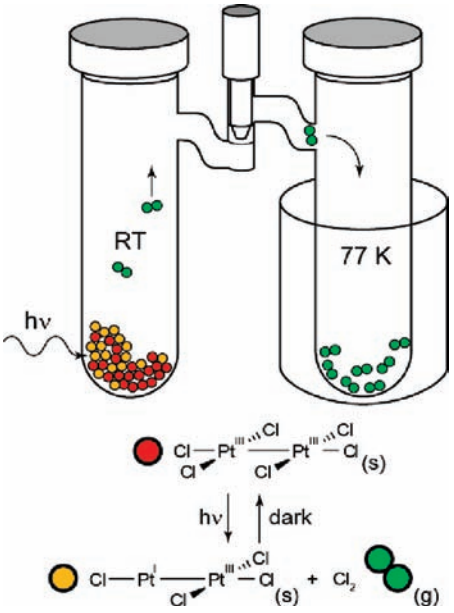

Figure 10. Schematic of the apparatus used to perform solid-state photoelimination of halogen gas from bimetallic Pt_2(tfepma) and Au_2(bisphosphine) complexes. The reactants and photoproducts are color-coded.

mations,[89] a four-electron photoreduction of halogen from $Au_2^{III,III}PP$ complexes proceeds as follows:

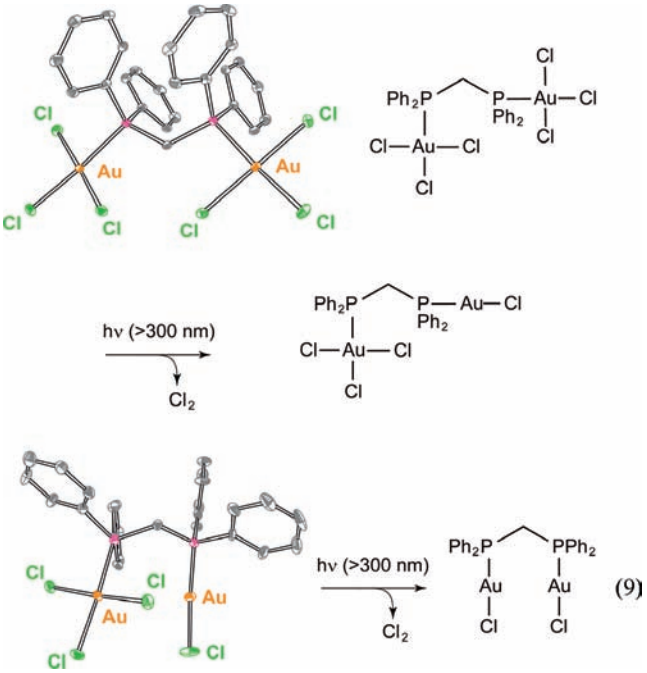

(9)

As with diplatinum compounds, the reaction occurs smoothly in the solid state in the absence of a trap; the X_2 back-reaction is prevented by virtue of the production of a volatile X_2 photoproduct.

With X_2 photoelimination realized, the stage is set to unify H_2 and X_2 photochemistry of two-electron mixed valency in a single system and thus furnish an authentic HX-splitting (X = halide) scheme. These studies are currently underway.

2.3. PCET. The activation of all energy-related molecules requires the coupling of electron equivalents to

(84) Esswein, A. J.; Dempsey, J. L.; Nocera, D. G. *Inorg. Chem.* **2007**, *46*, 2362.
(85) Cook, T. R.; Esswein, A. J.; Nocera, D. G. *J. Am. Chem. Soc.* **2007**, *129*, 10094.
(86) Cook, T. R.; Surendranath, Y.; Nocera, D. G. *J. Am. Chem. Soc.* **2009**, *131*, 28.
(87) Teets, T. S.; Nocera, D. G. *J. Am. Chem. Soc.* **2009**, *131*, 7411.
(88) Kadis, J.; Shin, Y.-g. S.; Dulebohn, J. I.; Ward, D. L.; Nocera, D. G. *Inorg. Chem.* **1996**, *35*, 811.
(89) Ronco, S.; Ferraudi, G. Excited State Redox Reactions of Transition Metal Complexes. In *Handbook of Photochemistry and Photobiology*; Nalwa, H. S., Ed.; American Scientific Publishers: Stevenson Ranch, CA, 2003; p 283.

proton equivalents. Without this coupling, large reaction barriers confront small-molecule conversion, thus imposing large overpotentials, and hence energy inefficiency. For instance, the H_2 half-reaction proceeds at 0 V vs NHE when the reaction proceeds in a discrete two-electron, proton-coupled step. If the electron and proton are uncoupled, then the reaction proceeds through a $H^{\bullet}$ radical and, consequently, confronts a barrier of 2.3 V vs NHE. The uncoupled one-electron/one-proton reactions to produce $HO^{\bullet}$ radicals are equally imposing. The challenge to lowering the activation barrier therefore arises in the intimate coupling of the electron and proton, prompting us to begin a research program targeting PCET reactions.

2.3.1. Mechanism of PCET. The coupling of a proton and electron has long been known in a thermodynamic sense, first explicitly defined to account for the pH dependence of redox couples.[90] In subsequent years, the kinetics of proton−electron coupling was inferred from free-energy relations and kinetic isotope effects of reactant to product conversions of enzymatic,[91,92] organic,[93−95] and inorganic substrates.[96,97] Notwithstanding, a predictable framework for PCET, at least to the extent that exists by way of the Marcus theory, was absent because the electron and proton had not been isolated in a PCET event. To this end, we turned our efforts toward isolating the PCET step and directly measuring the kinetics of the reaction. To do so, we created the uni- and bidirectional PCET networks shown in Figure 11.[98−100] The unidirectional D---[H^+]---A constructs (D = ET donor, A = ET acceptor, ---[H^+]--- = proton interface) provided tangible kinetic benchmarks for PCET reactions and stimulated the development of theories to describe PCET.[101,102] In these constructs, both the electron-transfer (ET) and proton-transfer (PT) distances are defined, with the caveat that the proton can be located anywhere within the interface. PCET is triggered by laser excitation of the donor or acceptor, and the PCET event is captured with time-resolved spectroscopy. Along its journey from donor to acceptor, the electron must negotiate the proton within the interface. Systems with symmetric interfaces such as cyclic carboxylic acid dimers[103] permitted the effect of the electronic coupling matrix element on PCET to be isolated, whereas

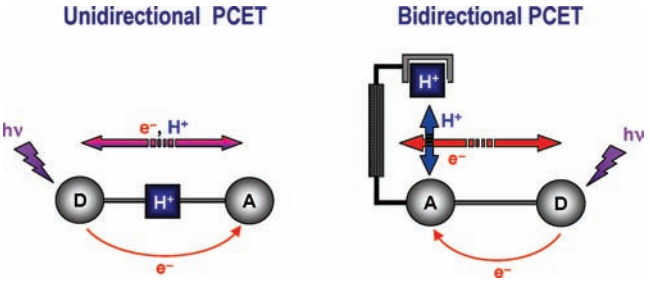

Figure 11. Supramolecular assemblies created to investigate PCET mechanisms for electron and proton transport along colinear and orthogonal pathways. In each system, the photoinduced electron transfer must negotiate the transfer of a proton. Reproduced from ref 8.

asymmetric interfaces, especially those composed of amidinium−carboxylate[104−110] and amidinium−sulfonate interactions,[112−114] permitted the effect of the Franck−Condon term on PCET to be defined.[115] From these studies, it was found that the distinguishing characteristic of a PCET reaction arises from the response of the polarization of the surrounding environment to the motion of the electron *and* proton.

At a mechanistic level, PCET fundamentally differs from traditional hydrogen atom transfer (HAT).[116] In a traditional HAT, the electron originates from the X−H bond (typically σ) and transfers colinearly with the proton to become part of the new H−Y bond. From the perspective of PCET, it is reasonable for the electron and proton to transfer adiabatically in a synchronous manner. However, in the PCET reactions of small molecules at metal active sites, the electron and proton are often site-differentiated and, consequently, considerable charge separation may accompany the activation reaction. This is especially true of water activation, where the proton is transferred to the oxo ligand with concomitant reduction of the metal. Though electron and proton movement may not originate or terminate at the same point, the proton can affect the electron transport. Furthermore, the same electron and proton do not have to couple throughout an entire transformation. As the electron moves, it may encounter different protons. All that is required for a

(90) Pourbaix, M. *Atlas of Electrochemical Equilibria in Aqueous Solutions*; Pergamon Press: Oxford, U.K., 1966.
(91) Klinman, J. P. *Philos. Trans. R. Soc. London B* **2006**, *361*, 1323.
(92) Kohen, A.; Klinman, J. P. *Acc. Chem. Res.* **1998**, *31*, 397.
(93) Wiberg, K. B. *Chem. Rev.* **1955**, *55*, 713.
(94) Westheimer, F. H. *Chem. Rev.* **1961**, *61*, 265.
(95) Scheppele, S. E. *Chem. Rev.* **1972**, *72*, 511.
(96) Mayer, J. M. *Annu. Rev. Phys. Chem.* **2004**, *55*, 363.
(97) Huynh, M. H. V.; Meyer, T. J. *Chem. Rev.* **2007**, *107*, 5004.
(98) Chang, C. J.; Brown, J. D. K.; Chang, M. C. Y.; Baker, E. A.; Nocera, D. G. In *Electron Transfer in Chemistry*; Balzani, V., Ed.; Wiley-VCH: Weinheim, Germany, 2001; Vol. *3.2.4*, p 409.
(99) Stubbe, J.; Nocera, D. G.; Yee, C. S.; Chang, M. C. Y. *Chem. Rev.* **2003**, *103*, 2167.
(100) Chang, C. J.; Chang, M. C. Y.; Damrauer, N. H.; Nocera, D. G. *Biophys. Biochim. Acta* **2004**, *1655*, 13.
(101) Cukier, R. I.; Nocera, D. G. *Annu. Rev. Phys. Chem.* **1998**, *49*, 337.
(102) Hammes-Schiffer, S. *Acc. Chem. Res.* **2001**, *34*, 273.
(103) Turró, C.; Chang, C. K.; Leroi, G. E.; Cukier, R. I.; Nocera, D. G. *J. Am. Chem. Soc.* **1992**, *114*, 4013.
(104) Yeh, C. Y.; Miller, S. E.; Carpenter, S. D.; Nocera, D. G. *Inorg. Chem.* **2001**, *40*, 3643.
(105) Damrauer, N. H.; Hodgkiss, J. M.; Rosenthal, J.; Nocera, D. G. *J. Phys. Chem. B* **2004**, *108*, 6315.
(106) Roberts, J. A.; Kirby, J. P.; Nocera, D. G. *J. Am. Chem. Soc.* **1995**, *117*, 8051.
(107) Roberts, J. A.; Kirby, J. P.; Wall, S. T.; Nocera, D. G. *Inorg. Chim. Acta* **1997**, *263*, 395.
(108) Deng, Y.; Roberts, J. A.; Peng, S. M.; Chang, C. K.; Nocera, D. G. *Angew. Chem., Int. Ed. Engl.* **1997**, *36*, 2124.
(109) Kirby, J. P.; Roberts, J. A.; Nocera, D. G. *J. Am. Chem. Soc.* **1997**, *119*, 9230.
(110) Kirby, J. P.; van Dantzig, N. A.; Chang, C. K.; Nocera, D. G. *Tetrahedron Lett.* **1995**, *36*, 3477.
(111) Rosenthal, J.; Young, E. R.; Nocera, D. G. *Inorg. Chem.* **2007**, *46*, 8668.
(112) Rosenthal, J.; Hodgkiss, J. M.; Young, E. R.; Nocera, D. G. *J. Am. Chem. Soc.* **2006**, *128*, 10474.
(113) Young, E. R.; Rosenthal, J.; Nocera, D. G. *Chem. Commun.* **2008**, 2322.
(114) Young, E. R.; Rosenthal, J.; Hodgkiss, J. M.; Nocera, D. G. *J. Am. Chem. Soc.* **2009**, *131*, 7678.
(115) Hodgkiss, J. M.; Damrauer, N. H.; Pressé, S.; Rosenthal, J.; Nocera, D. G. *J. Phys. Chem. B* **2006**, *110*, 18853.
(116) Hodgkiss, J. M.; Rosenthal J.; Nocera, D. G. In *Handbook of Hydrogen Transfer. Physical and Chemical Aspects of Hydrogen Transfer*; Hynes, J. T., Klinman, J. P., Limbach, H.-H., Schowen, R. L., Eds.; Wiley-VCH: Weinheim, Germany, 2006; Vol. *2.4.17*, p 503.

PCET event is that the kinetics and thermodynamics of electron transport depend on the position of a specific proton or a set of protons at any given time. Nevertheless, the protons and electrons must couple; if they do not, then large kinetic barriers are imposed on the activation reaction.

PCET is intrinsically a quantum mechanical effect because both the electron and proton tunnel as a result of the overlap between the donor and acceptor wavefunctions.[117,118] The proton rest mass is ~2000 times that of the electron and, as such, the proton wavelength is ~40 times shorter than that of an electron at a fixed energy. Consequently, PT is fundamentally limited to short distances, whereas the electron, as the lighter particle, may transfer over much longer distances. For this reason, the unidirectional PCET networks impose an inherent limitation on controlling the length-scale disparity between PT and ET because the network is assembled by the hydrogen bonds of the proton interface. PT distances are therefore confined to the hydrogen-bond length scale imposed by the ---[H^+]--- bridge.

Conversely, bidirectional PCET networks afford a facile means to manage the disparate length scales of the electron and proton.[119,120] The bidirectional PCET model systems schematically represented in Figure 11 orthogonalize the ET and PT coordinates. The PT distance is established by a rigid scaffold that poises an acid−base group above an ET conduit. In these "Hangman" architectures, a carboxylic acid or amidine is positioned over porphyrin[121−124] or salen[125−127] platforms via a xanthene or dibenzofuran spacer. When an electron acceptor or donor is appended to the redox platform, a PCET reaction may be established with PT to or from the hanging group. The Hangman constructs allow for the incisive investigation of the role of proton tunneling in PCET because the PT distance may be independently adjusted from the ET distance.[128]

2.3.2. Hangman and Pacman Porphyrins for the PCET Activation of Oxygen. We have shown that bidirectional PCET at Hangman platforms can be exploited to activate O−O[129] bonds, from which catalysis may be derived.[130−136] Proton transfer from the acid−base hanging group in M^{III} (M = Fe or Mn) Hangman porphyrin and salen peroxide complexes yields high-valent metal−oxo intermediates via exclusive $2e^-$ bond heterolysis.[137,138] Homolytic O−O bond cleavage, a $1e^-$, $1H^+$ transformation, is circumvented by coupling a single proton to drive the $2e^-$ heterolytic bond-cleavage event.

The electrophilic oxo of the Hangman platform exhibits reactivity patterns essential for water activation.[139,140] The oxo reacts with peroxide, which dismutates to O_2 and H_2O, and it is also present as a crucial intermediate in the reduction of O_2 to H_2O. This latter transformation is important to our goals of developing solar fuel chemistry because the conversion is the microscopic reverse of the O−O bond-forming chemistry that is needed for water splitting. Specifically, we have used the O_2 reduction chemistry of Pacman dicobalt(II,II) bisporphyrins as a roadmap to water splitting.[141] Oxygen is efficiently reduced to water within the Pacman cleft but only if a proton is present. Proton transfer to the $[Co_2O_2]^+$ superoxo core of $[Co_2^{III,III}$(bisporphyrin)$(O_2)]^+$ triggers a two-electron transfer. If the superoxo is insufficiently basic, one-electron reduction of $[Co_2^{III,III}$(bisporphyrin)$(O_2)]^+$ ensues in the absence of a proton and peroxide is produced. Thus, by coupling a proton to a multielectron transfer, the O−O bond is cleaved. The overall mechanism provides several valuable lessons for the design of a water-splitting catalyst. First, a high metal−oxo bond strength, and attendant kinetic barrier, is circumvented with the use of a late metal such as cobalt. Second, the 4 equiv needed for water splitting is afforded from a multimetallic active site. Finally, the use of protons is critical for O−O bond cleavage. Similarly, proper proton management may be expected to be critical to O−O bond formation.

3. Water Splitting Catalysis

With a framework in place for *multielectron* processes that are *proton-coupled* for the *activation of kinetically inert and thermodynamically stable bonds*, we turned our efforts to creating a water-splitting catalyst. Our design roadmap was influenced significantly by nature's approach to water splitting. In photosynthesis, water splitting is accomplished by the oxygen-evolving complex (OEC) of Photosystem II (PS II).[142,143] OEC splits water by first releasing oxygen to leave four electrons and four protons, which are then combined with $NADP^+$ (to NADPH) at the spatially remote site of ferredoxin-$NADP^+$ reductase (FNR), which resides in Photosystem I. Light is collected and converted by PS II into

(117) Hammes-Schiffer, S. *Acc. Chem. Res.* **2006**, *39*, 93.
(118) Reece, S. Y.; Nocera, D. G. In *Quantum Tunneling in Enzyme Catalyzed Reactions*; Scrutton, N., Allemann, R., Eds.; Royal Society of Chemistry Press: London, 2009.
(119) Reece, S. Y.; Hodgkiss, J. M.; Stubbe, J.; Nocera, D. G. *Philos. Trans. R. Soc. London B* **2006**, *361*, 1351.
(120) Reece, S. Y.; Nocera, D. G. *Annu. Rev. Biochem.* **2009**, *78*, 673.
(121) Yeh, C. Y.; Chang, C. J.; Nocera, D. G. *J. Am. Chem. Soc.* **2001**, *123*, 1513.
(122) Chang, C. J.; Chng, L. L.; Nocera, D. G. *J. Am. Chem. Soc.* **2003**, *125*, 1866.
(123) Chng, L. L.; Chang, C. J.; Nocera, D. G. *Org. Lett.* **2003**, *5*, 2421.
(124) Chang, C. J.; Yeh, C. Y.; Nocera, D. G. *J. Org. Chem.* **2002**, *67*, 1403.
(125) Liu, S.-Y.; Nocera, D. G. *J. Am. Chem. Soc.* **2005**, *127*, 5278.
(126) Yang, J. Y.; Bachmann, J.; Nocera, D. G. *J. Org. Chem.* **2006**, *71*, 8706.
(127) Yang, J. Y.; Nocera, D. G. *Tetrahedron Lett.* **2008**, *49*, 4796.
(128) Hodgkiss, J. M.; Krivokapić, A.; Nocera, D. G. *J. Phys. Chem. B* **2007**, *111*, 8258.
(129) Yang, J. Y.; Nocera, D. G. *J. Am. Chem. Soc.* **2007**, *129*, 8192.
(130) Chang, C. J.; Chng, L. L.; Nocera, D. G. *J. Am. Chem. Soc.* **2003**, *125*, 1866.
(131) Chng, L. L.; Chang, C. J.; Nocera, D. G. *Org. Lett.* **2003**, *5*, 2421.
(132) Rosenthal, J.; Chng, L. L.; Fried, S. D.; Nocera, D. G. *Chem. Commun.* **2007**, 2642.
(133) Liu, S.-Y.; Nocera, D. G. *Tetrahedron Lett.* **2006**, *47*, 1923.
(134) Yang, J. Y.; Nocera, D. G. *ChemSusChem.* **2008**, *1*, 941.
(135) Rosenthal, J.; Nocera, D. G. *Acc. Chem. Res.* **2007**, *40*, 543.
(136) Rosenthal, J.; Nocera, D. G. *Prog. Inorg. Chem.* **2007**, *55*, 483.
(137) Liu, S.-Y.; Soper, J. D.; Yang, J. Y.; Rybak-Akimova, E. V.; Nocera, D. G. *Inorg. Chem.* **2006**, *45*, 7572.
(138) Soper, J. D.; Kryatov, S. V.; Rybak-Akimova, E. V.; Nocera, D. G. *J. Am. Chem. Soc.* **2007**, *129*, 5069.
(139) Betley, T. A.; Wu, Q.; Voorhis, T. V.; Nocera, D. G. *Inorg. Chem.* **2008**, *47*, 1849.
(140) Betley, T. A.; Surendranath, Y.; Childress, M. V.; Alliger, G. E.; Fu, R.; Cummins, C. C.; Nocera, D. G. *Philos. Trans. R. Soc. London B* **2008**, *363*, 1293.
(141) Chang, C. J.; Loh, Z.-H.; Shi, C.; Anson, F. C.; Nocera, D. G. *J. Am. Chem. Soc.* **2004**, *126*, 10013.
(142) Barber, J. *Philos. Trans. R. Soc. London A* **2007**, *365*, 1007.
(143) Barber, J. *Inorg. Chem.* **2008**, *47*, 1700.

a wireless current, which is fed to OEC and FNR catalytic sites so that they can perform water splitting. Outside of the leaf, solar fuels other than hydrogen may be produced with the protons and electrons extracted from water, including the reduction of CO_2 to methanol. However, all water-splitting schemes require oxygen production, and the efficiency of this step is the singular primary impediment toward realizing artificial photosynthesis.[144]

In addressing the creation of a water-splitting catalyst, we applied several design constraints. Foremost among these was that the catalyst operates in water under ambient environmental conditions. This constraint presented two significant challenges. First, water is a poor proton acceptor under neutral conditions. Hence, the activation of oxygen in water required us to implement a bidirectional PCET based on our studies of radical transport in ribonucleotide reductase.[99,118,145,146] We showed that the oxygen of tyrosine could be activated in neutral water by the MLCT excited state of rhenium polypyridyl, but only if HPO_4^{2-} is present.[119,147,148] The reaction kinetics are pH-dependent and consistent with a PCET mechanism in which electron transfer from tyrosine to the photooxidant is accompanied by a bidirectional proton transfer from the oxygen of tyrosine to HPO_4^{2-}. Accompanying theoretical work on the model system supported such a concerted PCET mechanism, with HPO_4^{2-} acting as the proton acceptor.[149] Second, the splitting of neutral water presents the additional challenge that catalysts are notoriously unstable under such conditions. Except precious metal oxides,[150] the best proton acceptor is typically the catalyst itself and hence the protons produced from water splitting often promote corrosion of the catalyst. Consequently, any successful water-splitting catalyst must be self-healing.

3.1. Molecule-Based Water-Splitting Catalyst. The goal of producing a molecular water-splitting catalyst has occupied chemistry for several decades.[144] On the basis of the foregoing results of sections 2.3.2 and 3, studies were undertaken to design a water-splitting catalyst based on cobalt and phosphate (Pi).[151] Our efforts were rewarded with a catalyst that self-assembles from aqueous solution upon oxidation of Co^{2+} to Co^{3+}. A phosphate anion manages the protons released from water oxidation and also provides a mechanism for repair. The cobalt OEC (Co-OEC) is the first catalyst to operate in neutral water and hence enables the inexpensive and efficient generation of hydrogen and oxygen from water. Co-OEC is unique because it (1) operates safely with high activity under benign conditions (room temperature and pH 7), (2) is comprised of inexpensive, earth-abundant materials and is easy to manufacture and engineer, (3) is self-healing, (4) is functional in natural water streams and seawater, (5) can form on diverse conducting surfaces of varying geometry and therefore can be easily interfaced with a variety of light-absorbing and charge-separating materials, and (6) may be activated by solar-derived electricity or directly by sunlight mediated by a semiconductor.

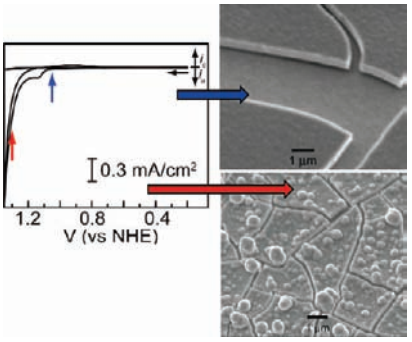

Figure 12. Cyclic voltammogram of an aqueous solution containing 1 mM Co^{2+} and 0.1 M Pi electrolytes. Scanning electron microscopy images are shown of catalyst films that form when the electrode is held at the indicated precatalytic and catalytic potentials.

3.1.1. Active and Highly Manufacturable. The Co-OEC forms in situ upon controlled potential electrolysis of Co^{2+} salts in pH 7 phosphate (Pi), methylphosphonate (MePi), or borate (Bi) electrolytes.[151,152] During this time, a dark-green-black film forms on the surface of the electrode surface. The catalyst deposits on a diverse array of conductive substrates (e.g., metals, indium−tin oxide, fluorinated tin oxide, etc.) and films with thicknesses of 1−3000 nm may be grown depending on the electrodeposition time. Extremely smooth catalytically active films form immediately following oxidation of Co^{2+} to Co^{3+} (see Figure 12). This potential is more similar to the $Co^{3+/2+}$ couple for a cobalt ion with hydroxo ligands as opposed to aqua ligands ($E[Co(OH)_2^{+/0}]$ = 1.1 V vs NHE and $E[Co(OH_2)_6^{3+/2+}]$ = 1.9 V vs NHE[153]). Roughened films are obtained if the potential is stepped into the catalytic wave. All film morphologies, smooth or roughened, are active catalysts. Dissolved cobalt is not needed for catalyst operation, and catalyst films are stable under normal storage conditions. The mild aqueous electrodeposition conditions permit a conformal catalyst layer to form on complicated architectures.

Co-OEC rivals or outperforms other water oxidation catalysts at neutral pH. The catalyst operates at 350 mV lower overpotential than platinum at all current densities at pH 7 (Figure 13). When operated at 10 mA/cm^2, Co-OEC also outperforms expensive RuO_2 anodes,[154] widely considered to be a superior OEC.[150] Moreover, the uniquely benign operating conditions translate into a new class of water-splitting technologies that perform under safe conditions with low material and engineering costs. All-plastic composite electrolyzer cells have been constructed with cheap membranes and electrode materials.

(144) Eisenberg, R.; Gray, H. B. *Inorg. Chem.* **2008**, *47*, 1697.
(145) Seyedsayamdost, M. R.; Yee, C. S.; Reece, S. Y.; Nocera, D. G.; Stubbe, J. *J. Am. Chem. Soc.* **2006**, *128*, 1562.
(146) Seyedsayamdost, M. R.; Reece, S. Y.; Nocera, D. G.; Stubbe, J. *J. Am. Chem. Soc.* **2006**, *128*, 1569.
(147) Reece, S. Y.; Nocera, D. G. *J. Am. Chem. Soc.* **2005**, *127*, 9448.
(148) Irebo, T.; Reece, S. Y.; Sjödin, M.; Nocera, D. G.; Hammarström, L. *J. Am. Chem. Soc.* **2007**, *129*, 154622.
(149) Ishikita, H.; Soudackov, A. V.; Hammes-Schiffer, S. *J. Am. Chem. Soc.* **2007**, *129*, 11146.
(150) The Electrochemistry of Novel Materials. In *Frontiers of Electrochemistry*; Lipkowski, J. Ross, P. N., Eds.; VCH: New York, 1994; Vol. *3*, and references cited therein.
(151) Kanan, M. W.; Nocera, D. G. *Science* **2008**, *321*, 1072.
(152) Surendranath, Y.; Dincă, M.; Nocera, D. G. *J. Am. Chem. Soc.* **2009**, *131*, 2615.
(153) Brunschwig, B. S.; Chou, M. H.; Creutz, C.; Ghosh, P.; Sutin, N. *J. Am. Chem. Soc.* **1983**, *105*, 4832.
(154) Burke, L. D.; Murphy, O. J.; O'Neill, J. F.; Venkatesan, S. *J. Chem. Soc., Faraday Trans. 1* **1977**, *73*, 1659.

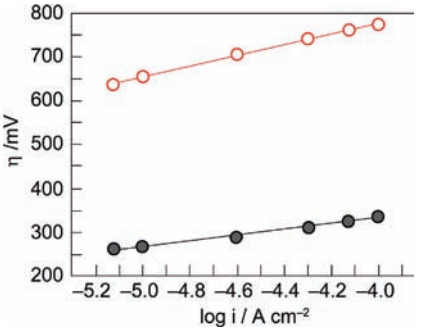

Figure 13. Tafel plots showing higher water oxidation activity of Co-OEC (●, gray) at lower overpotentials relative to platinum (○, red) in aqueous solutions containing phosphate.

Current densities as large as 60 mA/cm^2 have been achieved at 250 mV overpotential from neutral water at room temperature; current densities approaching 100 mA/cm^2 have been observed from these plastic composite electrolyzer cells at temperatures operating at 60 °C.

3.1.2. Molecular Cubane. Extended X-ray absorption fine structure (EXAFS) and X-ray absorption near-edge structure (XANES) spectra have been measured on isolated Co-OEC films[155] and Co-OEC films undergoing active catalysis.[156] In its resting state, the film is primarily composed of Co^{3+} ions and a minority population of Co^{2+} ions. Upon application of a potential, the appearance of Co^{4+} is evident in electron paramagnetic resonance and XANES spectra. Despite the presence of Co^{2+}, Co^{3+}, and Co^{4+}, the EXAFS spectrum, which is identical for films in resting or active states, exhibits two prominent peaks at 1.89 Å for d(Co−O) and at 2.81 Å for d(Co−Co). The EXAFS spectrum is noticeably different from those of solid state oxides including Co_3O_4, CoO, and CoO(OH), which exhibit prominent scattering features at longer distances (>4 Å) because of focusing effects arising from Co---Co---Co vectors in extended solids. Simulations of the EXAFS spectrum and analysis of model compounds reveal that Co-OEC is composed of Co-oxo cubanes; nearest-neighbor metal−metal interactions of 3.6 Å indicate the presence of connected incomplete $Co_3(\mu\text{-}O)_4$ or complete $Co_4(\mu\text{-}O)_4$ dicubane units. A proposed structure of the catalyst in its resting state is shown in Figure 14.

3.1.3. Self-Healing Catalyst. Non-noble metal oxide catalysts corrode under benign conditions because of the protons produced by water oxidation. In neutral water, the best base is the metal oxide itself, and consequently the very process of water-splitting hastens catalyst corrosion. For the case of Co-OEC, the involvement of Co^{2+}, Co^{3+}, and Co^{4+} oxidation states during catalysis presents an additional challenge to the design of a robust catalyst. Co^{2+} is a high-spin ion and is substitutionally labile, whereas Co^{3+} and Co^{4+} are low-spin and substitutionally inert in an oxygen-atom ligand field. Because the propensity of metal ion dissolution from solid oxides has been shown to correlate with ligand substitution rates,[157] Co-OEC is expected to be structurally

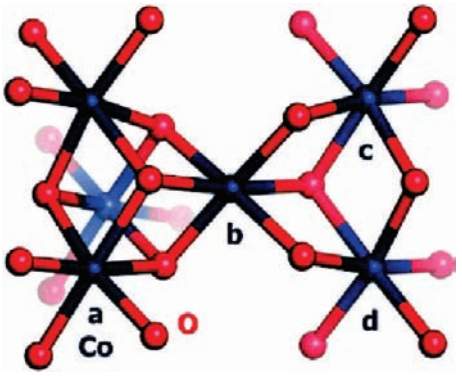

Figure 14. Proposed dicubane structure of the Co-OEC (cobalt in blue and oxygen in red) based on the XAS experiments of ref 155. Reproduced from ref 155.

unstable during turnover. Notwithstanding, Co-OEC is robust because of its unique ability to undergo self-repair.[158]

By monitoring radioactive isotopes of films composed of ^{57}Co and ^{32}P during water-splitting catalysis, we have shown that cobalt and phosphate are in a dynamic equilibrium during turnover. As shown in Figure 15a, any $^{57}Co^{2+}$ released into solution during water-splitting catalysis is redeposited upon its oxidation to Co^{3+} in the presence of phosphate. An equilibrium between Co^{3+} and Pi causes the cobalt cubane clusters to re-form during catalysis. This result accords well with the in situ formation of Co-OEC upon oxidation of Co^{2+} to Co^{3+} (vide infra). Figure 15b additionally shows that phosphate exchange is significantly greater than that of cobalt, as expected based on the molecular structure of the catalyst. The release of phosphate from a terminal ligation site should be much more facile than the release of a cobalt ion that is a constituent of a metal−oxo cubane core.

The "reversible corrosion" process engenders long-term stability of Co-OEC. Moreover, the repair mechanism can be used to "rescue" metal oxide catalysts that have corroded. As shown in Figure 15c, typical cobalt oxide water-splitting catalysts rapidly corrode under applied potentials that support water oxidation. The corrosion process is reversed immediately upon the addition of Pi and Co-OEC film forms as an overlayer to the corroding cobalt oxide film. The current stabilizes and water splitting proceeds with the characteristics of Co-OEC.

3.1.4. Water Splitting from Natural Water Sources. Co-OEC does not require pure water to function. This behavior is in contrast to catalysts in commercial electrolyzers, which require very high-purity water as an input stream (typically to 18 MΩ). Oxygen production by Co-OEC from salt water (0.5 M Cl^-) and seawater is accompanied by negligible levels of chlorine or hypochlorite.[152] This is in contrast to typical metal oxide water-splitting catalysts, which promote Cl^- oxidation in preference to water splitting. More recently, Co-OEC has been shown to produce oxygen selectively from natural river streams. Figure 16 shows that the activity

(155) Risch, M.; Khare, V.; Zaharieva, I.; Gerencser, L.; Chernev, P.; Dau, H. *J. Am. Chem. Soc.* **2009**, *131*, 6936.
(156) Kanan, M. W.; Surendranath, Y.; Dincă, M.; Yano, J.; Yachandra, V. K.; Nocera, D. G., to be published.
(157) Casey, W. H. *J. Colloid Interface Sci.* **1991**, *146*, 586.
(158) Lutterman, D. A.; Surendranath, Y.; Nocera, D. G. *J. Am. Chem. Soc.* **2009**, *131*, 3838.

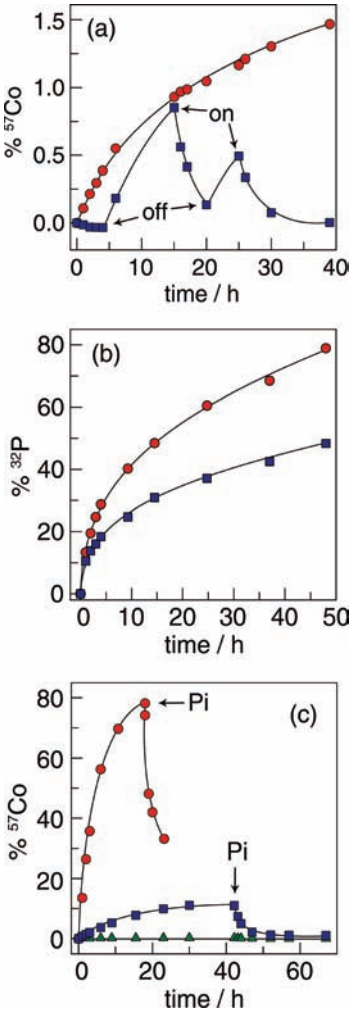

Figure 15. Radioactive isotope tracer studies of the Co-OEC repair process. (a) Percentage of ^{57}Co leached from films of Co-OEC on an electrode: with a potential bias of 1.3 V (NHE) turned on and off at the times designated (■, blue) (the trace begins with the applied potential on) and without an applied potential bias (●, red). (b) ^{32}P leaching from Co-OEC on an electrode with an applied potential of 1.3 V (NHE) (■, blue) and without an applied potential bias (●, red). (c) Percentage of ^{57}Co leached from a typical cobalt oxide catalyst on an electrode under potential biases of 1.3 V (■, blue) and 1.5 V (●, red) (NHE) and on an unbiased electrode (▲, green). Pi was added at the time points indicated by the arrows. Adapted from ref 158 and reproduced here with permission from the American Chemical Society.

of Co-OEC in water from the Charles River passing in front of MIT parallels the activity of the catalyst in highly pure water with only a 40 mV offset. The efficient oxygen-evolving ability of Co-OEC in seawater and natural water provides a significant technological advantage for the design of inexpensive electrolyzers interfaced to photovoltaic devices. We believe that the ability of Co-OEC to operate on natural water supplies is intimately connected to the repair mechanism. The catalyst does not foul because it breaks down and re-forms during catalysis. Hence, a fresh catalyst surface is continually being presented during water splitting.

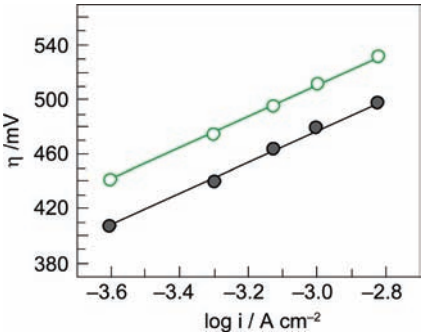

Figure 16. Tafel plots for Co-OEC in 18 MΩ water (●, gray) and water collected from the Charles River in front of MIT (○, green).

3.1.5. Photoelectrolysis. The generality and mildness of Co-OEC formation opens new avenues of exploration for solar fuel storage. Because water splitting is not performed in highly acidic or basic conditions, Co-OEC is amenable to integration with charge-separating networks comprising protein[159] and organic and inorganic[160−162] constituents. In these systems, the one-photon, one-electron charge separation can be accumulated by the catalyst to attain the 4 equiv needed for water splitting. The benefits of this approach have already been demonstrated for direct light-to-fuel conversion by forming Co-OEC on inexpensive light-harvesting anodes of a photoelectrochemical cell (PEC).[163] Co-OEC formation on mesostructured α-Fe_2O_3 results in a >350 mV cathodic shift of the onset potential for PEC water oxidation and significantly higher incident photon-to-current efficiencies than those observed for native α-Fe_2O_3. As demonstrated by this study, the ease of implementation of Co-OEC with a diverse array of photoactive materials suggests that the catalyst will be of interest to many in their endeavors to store solar energy by water splitting.[164]

3.2. Artificial Photosynthesis. Co-OEC captures many of the elements of the OEC of natural photosynthesis. Parallels between the two systems are highlighted in Chart 2.[165] The photosynthetic OEC is a distorted manganese−calcium−oxo cubane[166−169] that self-assembles upon light-driven oxidation of Mn^{2+} to Mn^{3+} in aqueous solution.[170] Similarly, the cobalt−oxo cubane of Co-OEC self-assembles upon oxidation of Co^{2+} to Co^{3+} in aqueous solution. Water oxidation in the photosynthetic membrane proceeds under ambient environmental

(159) Shih, C.; Museth, A. K.; Abrahamsson, M.; Blanco-Rodriguez, A. M.; Di Bilio, A. J.; Sudhamsu, J.; Crane, B. R.; Ronayne, K. L.; Towrie, M.; Vlcek, A., Jr.; Richards, J. H.; Winkler, J. R.; Gray, H. B. *Science* **2008**, *320*, 1760.

(160) Fukuzumi, S. *Phys. Chem. Chem. Phys.* **2008**, *10*, 2283.
(161) Hambourger, M.; Moore, G. F.; Kramer, D. M.; Gust, D.; Moore, A. L.; Moore, T. A. *Chem. Soc. Rev.* **2009**, *38*, 25.
(162) Flamigni, L.; Collin, J.-P.; Sauvage, J.-P. *Acc. Chem. Res.* **2008**, *41*, 857.
(163) Zhong, D. K.; Sun, J.; Inumaru, H.; Gamelin, D. R. *J. Am. Chem. Soc.* **2009**, *131*, 6086.
(164) Turner, J. *Nat. Mater.* **2008**, *7*, 770.
(165) Kanan, M. W.; Surendranath, Y.; Nocera, D. G. *Chem. Soc. Rev.* **2009**, *38*, 109.
(166) Ferreira, K. N.; Iverson, T. M.; Maghlaoui, K.; Barber, J.; Iwata, S. *Science* **2004**, *303*, 1831.
(167) Loll, B.; Kern, J.; Saenger, W.; Zoun, A.; Biesiadka, J. *Nature* **2005**, *438*, 1040.
(168) Yano, J.; Kern, J.; Sauer, K.; Latimer, M. J.; Pushkar, Y.; Biesiadka, J.; Loll, B.; Saenger, W.; Messinger, J.; Zouni, A.; Yachandra, V. K. *Science* **2006**, *314*, 821.
(169) Guskov, A.; Kern, J.; Gabdulkhakov, A.; Broser, M.; Zouni, A.; Saenger, W. *Nat. Struct. Mol. Biol.* **2009**, *16*, 334.
(170) Burnap, R. L. *Phys. Chem. Chem. Phys.* **2004**, *6*, 4803.

Chart 2. Comparison of the Functional Properties of the PS II OEC and Co-OEC

	Photosystem II OEC	*Co-OEC*
Self-Assembly	earth-abundant metal (Mn) all oxo core self-assembled from water by oxidation of Mn^{2+} to Mn^{3+}	earth-abundant metal (Co) all oxo framework self-assembled from water by oxidation of Co^{2+} to Co^{3+}
Repair	D1 protein	HPO_4^{2-}/Co^{3+} equilibrium
O_2 Generation	from neutral water at 1 atm and RT at low overpotential proton carrier (amino acids)	from neutral water at 1 atm and RT at low overpotential proton carrier (HPO_4^{2-})
Structure	a Mn-oxo cubane d(Mn–Mn) = 2.8 Å d(Mn–O) = 1.9 Å	a Co-oxo cubane d(Co–Co) = 2.8 Å d(Co–O) = 1.9 Å

conditions as it does for Co-OEC. In photosynthesis, PCET at the OEC is bidirectional. Proton transfer occurs along water channels defined by amino acid side chains that establish a PT pathway that is orthogonal to the ET pathway to and from the OEC.[171] For Co-OEC, a bidirectional PCET is established with Pi (or MePi or Bi) in order to manage the protons for PCET activation of the water molecules bound to the Co-OEC cubane. Oxygen production is harsh to the biological milieu; hence, the OEC−protein complex is structurally unstable, and a repair mechanism is required. Water oxidation at OEC produces reactive oxygen species, which damage the associated proteins of the PS II complex. Oxygenic photosynthetic organisms have evolved to replace the D1 protein in which the OEC resides with a newly synthesized copy every ~30 min.[172] Thus, functional stability is maintained despite structural instability. The same is true for Co-OEC. Though the catalyst is inherently unstable, a small overpotential enables the establishment of an equilibrium between Co^{3+} and Pi (MePi or Bi) that reverses the corrosion process specific to the Co^{2+} ion. Despite the structural instability of Co-OEC, function is preserved and oxygen is produced at a steady and reproducible rate.

Finally, the structural similarity of Co-OEC and the natural OEC is striking. Both water-splitting catalysts show only two prominent peaks in the EXAFS spectrum at 1.8 and 2.8 Å for the metal−oxo and metal−metal distances, respectively. On the basis of this structural similarity and the relationship between Co-OEC and OEC listed in Chart 2, one may ask whether cobalt could be accommodated in the OEC of a photosynthetic organism. Metal uptake experiments into higher order plants involving a variety of metals including cobalt have previously been attempted to no avail;[173] only manganese was observed to be taken into the OEC of PS II. However, metal uptake involving cobalt should be performed under low-light (LL) conditions. Photosynthetic organisms are known to downregulate metabolism under high-light (HL) conditions because of a variety of factors including oxygen toxicity.[174−176] In view of the high water-splitting activity of the cobalt cubane, it is not surprising that cobalt is toxic to the plant under HL conditions. However, would the same result be observed under LL conditions? More precisely, could photosynthetic organisms that exist under LL conditions, such as deep sea algae,[177] take advantage of a highly active OEC that is non-manganese-based? It is intriguing to note that some photosynthetic organisms that exist under LL conditions have an absolute cobalt requirement.[178] Whereas the organisms have cobalt-based cofactors (e.g., vitamin B_{12}), calculations of quotas suggest that a significant cobalt equivalency is unaccounted for by the presence of the cofactors.[179,180] These observations, together with the structural similarity of cobalt and manganese cubanes, point to the fascinating possibility that cobalt may be taken up into the OEC active site of photosynthetic organisms adapted for LL levels. Even if cobalt is not used naturally, LL photosynthetic organisms may be promiscuous in accepting cobalt (and other first-row metals such as nickel) into their OEC, depending on the external environmental conditions of light level, temperature, and nutrient availability. Such a possibility would not only be invaluable for the design of photosynthetic organisms for bioenergy but could also be important to understanding how global environmental changes may affect carbon cycling.

(171) Murray, J. W.; Barber, J. *J. Struct. Biol.* **2007**, *159*, 228.
(172) Aro, E.-M.; Suorsa, M.; Rokka, A.; Allahverdiyeva, Y.; Paakkarinen, V.; Saleem, A.; Battchikova, N.; Rintamaki, E. *J. Exp. Bot. E* **2005**, *56*, 347.
(173) Ananyev, G. M.; Zaltsman, L.; Vasko, C.; Dismukes, G. C. *Biochim. Biophys. Acta* **2001**, *1503*, 52.
(174) Barber, J.; Andersson, B. *Trends Biochem. Sci.* **1992**, *17*, 61.
(175) Aro, E. M.; Virgin, I.; Andersson, B. *Biochim. Biophys. Acta* **1993**, *1143*, 113.
(176) Long, S. P.; Humphries, S.; Falkowski, P. G. *Annu. Rev. Plant Physiol.* **1994**, *45*, 633.
(177) Coleman, M. L.; Chisholm, S. W. *Trends Microbiol.* **2007**, *15*, 398.
(178) Saito, M. A.; Moffett, J. W.; Chisholm, S. W.; Waterbury, J. B. *Limnol. Oceanogr.* **2002**, *47*, 1629.
(179) Sunda, W. G.; Huntsman, S. A. *Limnol. Oceanogr.* **1995**, *40*, 1404.
(180) Wilhelm, S. W.; Trick, C. G. *Can. J. Microbiol.* **1995**, *41*, 145.

4. Concluding Remarks

PE is transformative in its scope to achieve a secure energy future, to provide economic equity to people of the nonlegacy world, and to stem the flow of nonanthropogenic sources of CO_2 into our environment. However, downscaling current technologies to the personal level will not be economically feasible. Most energy systems are incommensurate with the very nature of PE because they have been designed to operate at large scale and high efficiency, and thus significant costs are associated with the balance of systems on a small scale. Hence, the solution to solar PE will be one that begins with a blank sheet on which the discovery of PE will be written. New materials, new reactions, and new processes such as those afforded by Co-OEC are needed to permit PE to be an attractive economic alternative. If the cost of solar PE through discovery can be decreased, then the development of the nonlegacy world can occur within an energy infrastructure that is of the future and not the past. Considering that it is the 6 billion nonlegacy users that are driving the enormous increase in the energy demand by midcentury, a research target of solar PE provides the global society its most direct path to providing a solution for its sustainable energy future.

Acknowledgment. D.G.N. is indebted to the many students and co-workers who have performed the research described herein. He also acknowledges the NSF and NIH for long-term support of his fundamental research and the AFOSR, ARO, and DOE for supporting research of targeted interest. Finally, D.G.N. acknowledges the Chesonis Family Foundation for their long-term vision and support of basic science that addresses important challenges confronting our societal future.